Journal of
Nanoscience and Nanotechnology
Vol. 7, 1–29, 2007

REVIEW

Electrical Properties and Applications of Carbon Nanotube Structures

Prabhakar R. Bandaru*

Department of Mechanical and Aerospace Engineering, Materials Science Program, University of California, San Diego, La Jolla, CA 92093-0411, USA

The experimentally verified electrical properties of carbon nanotube structures and manifestations in related phenomena such as thermoelectricity, superconductivity, electroluminescence, and photoconductivity are reviewed. The possibility of using naturally formed complex nanotube morphologies, such as Y-junctions, for new device architectures are then considered. Technological applications of the electrical properties of nanotube derived structures in transistor applications, high frequency nanoelectronics, field emission, and biological sensing are then outlined. The review concludes with an outlook on the technological potential of nanotubes and the need for new device architectures for nanotube systems integration.

Keywords: Carbon Nanotubes, Y-Junctions, Electrical and Electronic Properties, Optical Properties, Thermoelectrics, Superconductivity, Electronic Structure, Review.

CONTENTS

1. INTRODUCTION

Carbon nanotubes (CNTs) have recently emerged as the wonder materials of the new century and are being considered for a whole host of applications[1] ranging from large scale structures in automobiles to nanometer scale electronics. In this paper we review some of the electrical properties of CNT based materials and consider their utility. In addition to the advantages conferred by miniaturization, carbon based nanoelectronics promise greater flexibility compared[2] to conventional silicon electronics, one example being the extraordinarily large variety of carbon structures exemplified in organic chemistry. Consequently, nanotubes are also considered as candidates for molecular electronics.[3] Several remarkable properties, peculiar to low dimensionality,[4] can be harnessed in CNT structures and gainfully employed.

This aim of this review, in addition to enumerating the electrical properties of CNT derived structures, is to encourage the integration of a diverse set of electrical phenomena into a multifunctional CNT based device. While large scale assembly of CNTs, at a level that would be impressive to a systems designer,[5] is still challenging it is the author's opinion that such a device would encourage applications where power savings, radiation hardness, and reduced heat dissipation are major considerations. In this paper, firstly, the structure and electrical properties of the basic CNT morphologies, i.e., single-walled and multi-walled CNTs (SWNTs and MWNTs, respectively) are discussed. This will include significant features of electrical

*Author to whom correspondence should be addressed.

transport, which impact interpretation of measurements and suitability in advanced electronics. Basic issues involving doping to control nanotube properties, methods of contact from *higher dimensional* contacts/environment, and sensitivity to ambient conditions are relevant topics of concern. The application of such properties to related phenomena of photoconductivity, thermoelectricity, and superconductivity are then briefly reviewed. A few examples which explicitly involve the electrical and chemical characteristics of CNTs, such as a change in electrical conductivity for biomolecular sensing, and field emission will be discussed. A most exciting aspect, the application of CNTs to nano-devices incorporating high frequency (THz scale) electronics will then be studied. In this context, the possibility of using CNTs as antennae to transmit/receive information at the nanoscale is an important consideration. The review will conclude with an outlook for the application of the electrical properties in future technology. This review also attempts to cover ground that has not been considered in other recent reviews[3, 6–11] of CNT electronics and electrical transport.

While electrical properties have been measured on nanotubes synthesized through a variety of methods, this review does not specifically address methods of synthesis and characterization of nanotubes. Excellent reviews on the topic of nanotube/nanofiber synthesis exist in literature.[12–14] Briefly however, SWNTs and MWNTs have been synthesis by various methods, e.g., by arc discharge and laser ablation methods, which seem to have a higher degree of structural perfection, due to the high temperatures (>3000 °C) involved in the synthesis.[10] Nanotubes are also grown through Chemical Vapor Deposition (CVD) at a lower temperature (<1000 °C) with a higher defect density, which in turn adversely affects the electrical and thermal characteristics along with the structural properties. An issue of outstanding importance for the practical application of nanotubes, indeed in nanotechnology itself—that of alignment and fabricating large scale arrays of nano-structured elements will also not be addressed in this paper. Several methods for obtaining nanotube arrays are being worked on and include, *viz.,* the use of
(i) electric fields,[15, 16]
(ii) dip-pen lithography,[17]
(iii) microfluidic techniques,[18]
(iv) individual catalyst patterning,[19] and
(v) mechanical transfer.[20]

However, none of the above is completely satisfactory for the goal of rapid and controlled placement of nanotube/s of defined length and chirality.

2. SINGLE-WALLED NANOTUBES (SWNT)

A SWNT is formed by wrapping a single sheet of graphite (graphene- Fig. 1(a)), seamlessly, into tubular forms (Fig. 1(b)). It is interesting to note that graphene, by itself, can be characterized as either a zero-gap semiconductor or a metal, since the density of states (DOS) is zero at the Fermi energy (E_F), and imparts those properties to a nanotube. It is also well known that the fundamental conducting properties of a graphene tubule depend on the nature of wrapping (chirality) and the diameter (typically, SWNTs have diameters in the range[21] 0.4 nm–2 nm).

2.1. Electronic Structure

The electronic band structure of a nanotube can be described by considering the bonding of the carbon atoms arranged in a hexagonal lattice. Each carbon atom ($Z = 6$) is covalently bonded to three neighbor carbons *via* sp^2 molecular orbitals. The fourth valence electron, in the p_z orbital, hybridizes with all the other p_z orbitals to form a delocalized π-band. As the unit cell of graphene has two carbon atoms an even number of electrons are contained in the basic nanotube structure, which consequently can be metallic/semiconducting.[22] Mintmire,[23] Hamada,[24] and Saito[25] predicted through tight-binding electronic structure calculations that the relationship between the coefficients (n_1 and n_2) of the translational vector $c_h = n_1a_1 + n_2a_2$, which connects two crystallographically equivalent sites, determines the conducting properties

Dr. Prabhakar R. Bandaru, Assistant Professor of Materials Science at U.C.-San Diego. After receiving his Ph.D. from U.C. Berkeley, Dr. Bandaru worked at Applied Materials Inc. as a Process Engineer, on the development of novel ferro-electric materials for non-volatile information storage. Subsequently, as a postdoctoral fellow in the Electrical Engineering department at UCLA, he conducted research in solid state quantum computing and communications. Dr. Bandarus research accomplishments span the areas of carbon nanotubes, semiconductors, and optics. He fabricated the first all carbon nanotube based transistor, based on a Y-junction form where the gate was self-contained. He is also credited with the solution of a fifty-year old problem regarding the phase stability of MnBi, used for high-density magneto-optic recording, and discovered the beneficial effect of a-hydroxy acids for defect free semiconductor surfaces. His current research interests include the development of novel nanoelectronics using carbon nanotubes, techniques for nano-patterning, nanophotonics, and single electron and single photon devices.

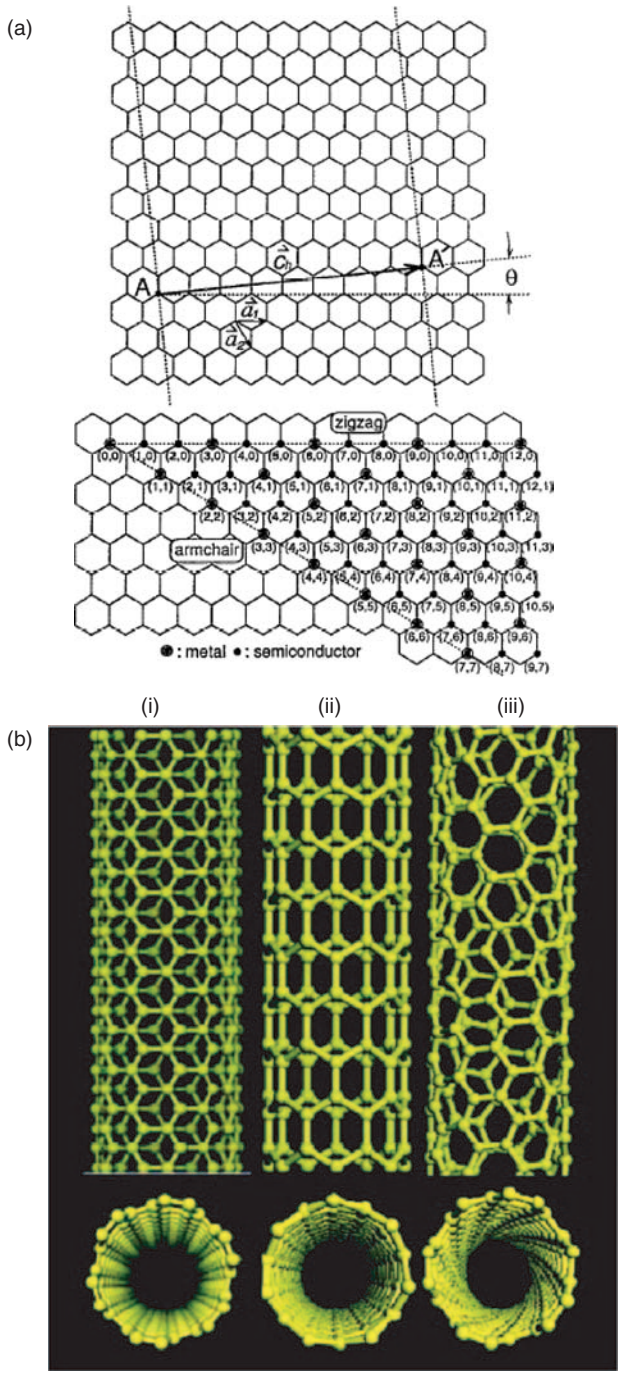

Fig. 1. (a) A single walled nanotube (SWNT) is formed by *wrapping* a graphene sheet into a cylinder with the nature of wrapping uniquely determined by the chiral vector $\mathbf{c_h}$. Either metallic/semiconducting SWNTs can be formed and account for the great variety of nanotube structures. Reprinted with permission from [25], R. Saito et al., *Appl. Phys. Lett.* 60, 2204 **(1992)**. © 1992, American Institute of Physics, (b) Illustrations of the structures of (i) Arm-chair, (ii) zig-zag, and (c) chiral SWNTs, and a multi-walled nanotube (MWNT) formed by telescoping several SWNTs, Reprinted with permission from [1], R. H. Baughman et al., *Science* 297, 787 **(2002)**. © 2002, Science Magazine.

(Fig. 1(b)). When 2 $n_1 + n_2$ is an integer multiple of three, the CNT exhibits metallic behavior while non-metallic/semiconducting behavior, with a band gap for conduction (E_g), is obtained in all other cases. (This can also be stated as: mod$(n_1 - n_2, 3) = 0, 1, 2$, where mod1 and mod2 SWNTS are semiconducting while mod0 SWNTS ($n_1 < n_2$) are metallic at room temperature, and exhibit a small chirality-dependent energy gap, corresponding to quasi-metallic conduction, at lower temperatures, the case $n_1 = n_2$ denotes armchair nanotubes that are truly metallic). If all values of the chiral vectors were equally probable, it would be expected that 1/3 of the total SWNTs would be metallic while the remaining 2/3 would be semiconducting, which is indeed what is found in synthesis.[21]

The Fermi level crossing for *zig-zag* $(n_1, 0)$ tubes, which can be metallic or semiconducting, is at the center of the Brillouin zone ($k = 0$). However, for *arm-chair* (n_1, n_1) tubes, the level crossings are at $k = \pm\frac{2\pi}{3a_o}$ and they are always metallic. It has also been found that for all *metallic* nanotubes, the E_F intersects two bands of the one-dimensional band structure corresponding to two modes of conduction (i.e., one with positive velocity and the other mode corresponding to oppositely moving electrons, with negative velocity)—this contributes a kinetic inductance to the nanotube, which has implications in the high frequency electronic properties of nanotubes (c.f., Section 8.1.3). Additionally, the requirement of maintaining periodicity around the circumference of the nanotube (of diameter d_t) causes quantization of the transverse wave-vector component ($k_\perp = \frac{2}{d_t}$), which dictates the allowed $k_\perp$ spacing of the sub-bands. Consequently, a large diameter nanotube will have many sub-bands while a smaller diameter tube will have fewer sub-bands. A more detailed discussion of the electronic band structure is found in Ref. [26] and references therein.

As can be seen from Figure 1(a) (ii), the nanotube diameter, dictated through $\mathbf{c_h}$, also affects the electron dispersion and it was derived[27] that in a semiconducting nanotube, $E_g = \frac{4\hbar v_F}{3d_t}$. The influence of the band structure topology (E_k) on the conduction is manifested through the relationship for the Fermi velocity $(v_F) = \hbar^{-1}\nabla_k \cdot E_k$. The above translates numerically[7] to $E_g = \frac{0.9}{d_t}$ eV, with a $v_F \sim 10^6$ m/s. The electronic structure, as represented through a density of states (DOS) diagram is found to exhibit characteristic $E^{-1/2}$ van Hove type singularities, typical of a one-dimensional system, and was well manifested in electrical[28] and optical measurements (see also Section 6). However, at the Fermi energy itself, for metallic nanotubes, the DOS is finite while for a semiconducting nanotube, the DOS is zero.

New physical principles are found to be necessary to explain nanotube phenomena. For example, the Fermi liquid theory which is used to describe electronic excitations, in the non-interacting electron limit, is found to be inadequate[29] to describe the electrical properties in SWNTs, in the one-dimensional limit. Compared to metals, in metallic nanotubes, the carrier density is lower by orders of magnitude and electron correlations will also have to

be considered. Consequently, the Luttinger liquid (LL) theory, which does take into account electron-electron interactions is more appropriate and can be embodied in novel phenomena[30] such as spin-charge separation, suppression of the electron tunneling density of states and interaction dependent power laws for the electrical conduction. In most experimental studies, however, the details of such behavior are masked by imperfect contacts and contact resistances. Theoretically, a g parameter which is the ratio of the single-electron charging energy to the single particle energy spacing is quoted for monitoring the degree of LL behavior in a one-dimensional system. In the *non-interacting* Fermi liquid case, $g = 1$, whereas interactions reduce the value of g. In SWNTs, g has been estimated to be in the range of ~0.2–0.3.[30] An experimental confirmation of such behavior in nanotubes/nanotube ropes[31] has been obtained through the power law dependence of the conductance (G) on voltage (V), i.e., $G\alpha V^{0.36}$ and temperature (T), i.e., $G\alpha T^{0.3-0.6}$. Further experimental confirmation of the LL behavior can also be made through tunneling experiments between two SWNTs.[32]

It is to be kept in mind, however, that the LL description strictly applies to metallic SWNTs[33] (Interestingly, it has been predicted[34] that in bundles of metallic SWNTs van der Waals interaction between individual nanotubes can induce a pseudo-gap of ~0.1 eV, which mimics semiconducting behavior).

2.2. Doping Characteristics of Nanotubes

For semiconducting SWNTs, in the absence of impurities or defects (doping), the Fermi energy (E_F) is taken to be at a reference value of zero. However, for a *realistic* graphene based nanotube a finite doping is inevitable due to the presence of adsorbates, from the ambient, which would cause charge transfer. In that case, the E_F is either <0 (for hole doping, electron transfer *from* the NT—p type) or >0 (for electron doping, electron transfer *to* the NT—n type). The effects of temperature also have to be taken into consideration i.e., (i) $k_B T > E_F$ or (ii) $k_B T < E_F$, (also see section 2.3). Case (i), suitable for high temperatures, corresponds to low doping while low temperatures (case (ii)) are typify strong doping conditions. In metallic nanotubes the results of the shifts in the Fermi level are masked by a higher density of states and doping effects are less marked.

When connected to external contacts, semiconducting SWNTs are usually measured to be p-type. This characteristic could be induced by the higher work function of the contact[35] whereby holes could be generated in the nanotube due to electron transfer from the NT to the contact. However, it was seen, in top-gated device structures with a field effect transistor (FET) configuration, that devices can show ambipolar characteristics[36] with larger drive currents. The device characteristics are then determined by the relative heights of the Schottky barrier for electron- and hole injection at the metal electrode-CNT interface. It was also determined[37] that the annealing in vacuum, through oxygen removal (or doping the surface with alkali metals) converts p-type devices to n-type, which results in a shift in the Fermi energy from the valence band to mid-gap. Interestingly, exposure to oxygen resulted in reversion to p-type characteristics. Evidence for charge transfer in doped carbon nanotube bundles exposed to electron donor (K, Rb) and electron acceptor (Br, I) atoms was also seen through Raman spectroscopy investgations[38] through a vibrational mode shift.

As mentioned earlier, it is seen that intrinsic nanotubes cannot be produced whenever there is exposure to oxygen ambients. The effect of oxygen on nanotubes is plausibly not just due to doping, as is conventionally understood but could be related more to the effects on the contacts. Also, the physisorbtion[39] of the oxygen with CNTs is weak and is unlikely to result in charge transfer. A phenomenological model was advanced to explain the p- to n-conversion (Fig. 2), where the concentration of oxygen is proportional to, and determines the position of, the E_F at the metal-CNT interface. Such an effect changes the line-up of the bands at the interface but does not involve the bulk of the CNT.

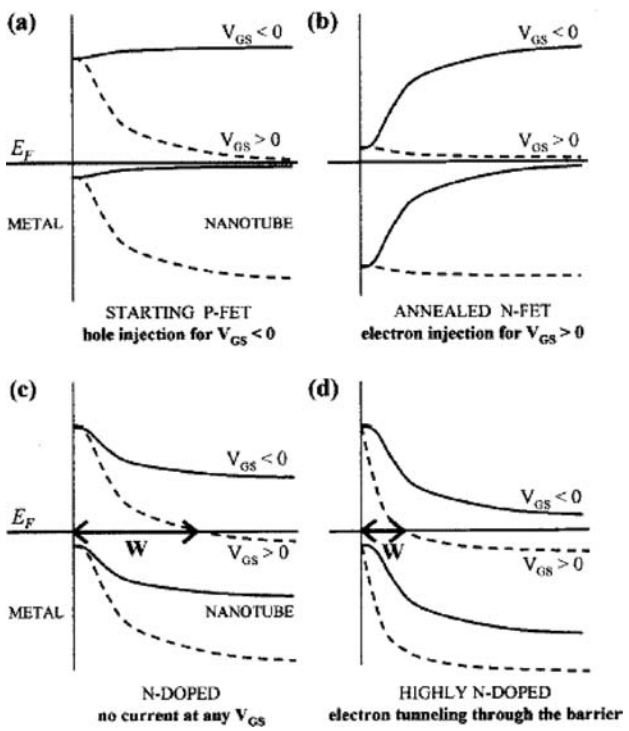

Fig. 2. Effect of ambient conditions on the electronic band structure of a CNT-metal contact. Initially, (a) the doping is p-type due to the higher work function of the metal *and* extrinsic oxygen doping, (b) When oxygen is driven out through an annealing treatment, the transistor behavior mimics a n-doped device in that electron injection is allowed, but (c) true n-type behavior is only obtained through alkali element (e.g., K) doping, (d) At higher doping levels, electron tunneling occurs through a thin barrier. Reprinted with permission from [37], V. Derycke et al., *Appl. Phys. Lett.* 80, 2773 **(2002)**. © 2002, American Institute of Physics.

When E_F at the junction is close to the center of the band gap, the barrier allows tunneling and ambipolar transport is observed. With Au contacts in air, only holes can be injected into the device, while annealing/removal of oxygen results in only electrons being injected due to the high hole injection barriers (Fig. 2(b)). Subsequently exposing the SWNTs to nitrogen[40] and alkali metal dopants[37] resulted in n-doping. However, in the latter case the strong oxidizing characteristics of the dopants are undesirable and stable doping can instead be obtained through functionalization by amine-rich polymers[12] such as polyethyleneimine (PEI).

Note that in a SWNT fabricated as a p-n junction, the depletion region is a dipole *ring*, c.f., as opposed to a dipole *sheet* in a planar junction.[41] Consequently, the depletion width (W) of a nanotube device at low doping levels is found to depend *exponentially* on the inverse doping fraction (f).[42] This factor needs to be considered in device design, where tunneling through the device occurs at $f > 2 \cdot 10^{-3}$ while in the opposite case, i.e., $f < 2 \cdot 10^{-4}$, a large depletion width is formed. Even outside the depletion region, the charge distribution is not cut-off abruptly, but has a logarithmic decay with distance z (as $\frac{1}{\ln(z/\lambda)}$, where λ is a constant proportional to the nanotube radius) and can extend up to μm distances. These limitations on charge confinement are intrinsic to nanotubes and demand a radical new design for devices. One might need to control the leakage current (in highly doped nanotube based p-n junctions, due to the large charge decay lengths) by including an undoped region of length (L) $\gg W$) between the p- and n-doped regions. This reduces the tunneling probability, and hence the leakage current, by an exponential factor, $\sim \exp(-2kL)$.

In summary, the mechanisms for doping and the determination of the acceptor and donor levels still need to be investigated. Raman spectroscopy, widely used for determining the metallic/semiconducting characteristics of nanotubes,[43] offers one possible way to determine the charge transfer characteristics through spectroscopic line shifts.[38, 44] Charged defects are also known[45] to modify electronic properties through local modification of the electronic structure (see also Sections 7.2 and 7.3(a)).

2.3. Characteristics of Electrical Transport

A determination of the band structure allows for the calculation of an energy dependent Drude conductivity (σ_{2D}) for the graphene sheet that constitutes a nanotube surface, as $= (\frac{2e^2}{h})\frac{E}{\hbar v_F} l_e$. The elastic scattering length (l_e) of the carriers is proportional to the electron-phonon scattering and generally increases with decreasing temperature (usually, $l_e \alpha\ T^{-p}$, with $p > 1$). One characterizes the electrical conductivity in two regimes:

(1) *Low temperatures* ($k_B T < E_F$), where in the conductivity equation above, the energy (E) replaced by E_F (the Fermi energy). The conductivity in this regime is *metallic*. A finite zero-temperature value, the magnitude of which is determined by the static disorder, is obtained.

(2) *High temperatures* ($k_B T > E_F$), where in the conductivity equation, the energy (E) is replaced by $k_B T$. The conductivity, and the carrier density, is then directly proportional to T.

At the very outset, it is not trivial to measure the intrinsic resistance of a SWNT. Any contact in addition to those at the two ends of the tube (say, for a four-terminal measurement) can destroy[46] the one-dimensional nature of the SWNT and make a true interpretation difficult. Theoretically, for a strictly one-dimensional system the Landauer formula predicts an intrinsic resistance (R^o_{int}), independent of the length, to be equal to $\frac{h}{e^2}\frac{1}{T(E_F)}$ which translates to a resistance of 25.8 kΩ) assuming perfect transmission through ideal Ohmic contacts, i.e., $T(E_F)$ equal to one. This *contact* resistance arises from an intrinsic mismatch between the external contacts to the wire (which are of higher dimensionality) and the one-dimensional nanotube system and is *always* present. When one takes individually into account both the two-fold spin and band degeneracy of a nanotube the intrinsic resistance (R_{int}) now becomes $\frac{h}{4e^2}\frac{1}{T(E_F)}$, which again seems to be length independent.

However, in the above discussion, we have not yet considered the contribution of the external contacts. When we consider the transmission (T) through the contacts into the one-dimensional channel and then to the next contact, $T = \frac{l_e}{l_e+L}$, where l_e is the mean free path length for scattering[46] and L is the length of the one-dimensional conductor. The resistance is now equal to

$$\frac{h}{4e^2}\frac{l_e + L}{l_e} \equiv \frac{h}{4e^2}\left(1 + \frac{l_e}{L}\right)$$

The first term represents R_{int} while the second term denotes an Ohmic resistance (R_{Ohmic}) associated with scattering. In the presence of dynamically scattering impurities, such as acoustical or optical phonons, which are inevitably present at any temperature above 0 K, the Ohmic resistance should definitely be considered. It is interesting to consider the limiting cases of a large mean free path ($l_e \to \infty$) or a small tube ($L \to 0$) i.e., in the ballistic regime, when the Ohmic resistance is seen to vanish. Finally, the material resistance of the contacts contributes an additional term: R_c. The total resistance as measured in an external circuit would now be: $R = R_{int} + R_{Ohmic} + R_c$. These considerations imply that a minimum resistance of $\frac{h}{4e^2}$ ($\sim$6.5 $k\Omega$) is present in a SWNT with a single channel of conduction. In practice however, imperfect contacts (which lead to $T < 1$) and the presence of impurities lead to larger resistance values, while deviations from strict one-dimensionality or multiple channels of conduction (as in a MWNT) could lead to smaller numbers for the resistance. These observations primarily account for the large discrepancy of the numerical value of the resistances in literature.

2.4. Experimental Measurements

For measuring the electrical properties, standard lithographic[47] practices are employed. A solution of SWNT ropes, dispersed in an organic solvent (e.g., dichloroethane), is spun onto an oxidized Silicon wafer. The nanotube is then aligned on to the electrodes (Source and Drain) either through Atomic Force Microscope (AFM) manipulation or electron-beam lithography alignment. Experiments are then typically carried out, in a three-terminal geometry (mimicking a FET—Field Effect Transistor topology) utilizing the Silicon wafer as a back-gate. Further details of experimental procedures are illustrated in Ref. [11].

The metallic/semiconducting characteristics of individual nanotubes are ascertained by the absence or dependence of the source-drain current-voltage characteristics on the gate voltage. While the smallest possible resistance of SWNTs is ∼6.5 kΩ, high contact/Ohmic resistances usually prevent the observation of such values. The granularity of the metal electrodes and contamination at the interface are some obstacles to the realization of good contacts. Several methods such as thermal and electron-beam induced annealing[48] are being attempted with moderate success. Early experimental results[35] on the I–V characteristics of semiconducting SWNTs (indicative of p-doping) in a FET like arrangement are shown in Figure 3. The pinning of the valence band of the nanotube to the Fermi level of the contact metal electrode (typically Au) results in the description of transport in the channel of the device as through two back-to-back connected Schottky barriers. The device operation can be explained by invoking band structure modification typical of a traditional semiconductor transistor.[41] The observed gain, in this case, was only ∼0.35 but could be increased by reducing the gate oxide thickness/using high κ-dielectrics.[49] The carrier mobility (μ) can be determined from the $(I–V_{bias})_{Vg}$ data[7] through

$$G = \frac{C'_g(V_g - V_{go})\mu}{L}$$

where C'_g is the capacitance per length (L) of the tube, and V_{go} is the threshold voltage. Owing to the nanotube-metal band alignment, it was found that the p-type (hole) conductance in nanotube FETs is higher than n-doped channels (electrons as majority carriers). While in the early experiments, hole mobilities of ∼200 cm^2/Vs were observed,[50] recent work[51] on longer nanotubes report mobilities exceeding 10,000 cm^2/Vs. Additionally, with Pd/Pt contacts, and *in situ* modification of the electrode work function through hydrogen annealing treatments,[52] Ohmic behavior has been induced with ballistic transport and measured nanotube resistance approaching the theoretical minimum of $R_o(=\frac{h}{4e^2})$. Such behavior, characteristic of reflection less contacts, were used to construct devices with perfect electron coherence, such as a Fabry-Perot interferometer.[53]

Further seminal work focused on low temperature transport in SWNTs, where non-linear transport characteristics such as Coulomb Blockade effects were observed.[54, 55] In this regime ($k_BT < E_F$), the nanotube is essentially behaving like a single-electron island (c.f., quantum dot)/array of islands, of very small capacitance (aF, $\sim 10^{-18}F$) where the addition of each extra electron results in an enormous charging energy ($=\frac{e^2}{2C}$) cost. A peak in the conductance corresponding to the addition of each extra electron has been observed as a function of the gate voltage[56] (Fig. 4). Further details of such experiments for observing quantum dot like behavior are found in Refs. [54, 57, 58], Such work has served to elucidate the nature of transport in nanotubes *vis-à-vis* resonant tunneling from the electrodes to discrete energy levels in the nanotubes and the coherence of electron currents, at low temperatures. However, significant deviations from the simple Coulomb blockade picture are mediated through the electronic correlations[59]

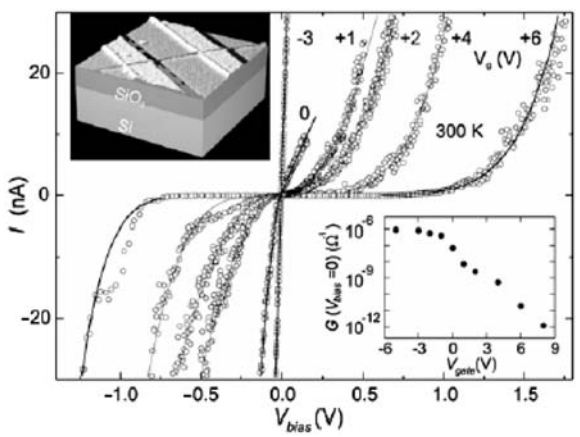

Fig. 3. Current–Voltage (I–V_{bias}) curves as a function of gate voltage (V_{gate}) reveal p-type characteristics for an SWNT arranged in a FET configuration (see top-left inset) The applied bias is across the source and drain electrodes (V_{bias}) and V_{gate} is applied on the backside of the FET. The decrease of the conductance (G) with increasingly positive V_{gate} (bottom-right inset) varies by six orders of magnitude and is characteristic of holes as majority carriers. Reprinted with permission from [35], S. J. Tans et al., *Nature* 393, 49 **(1998)**. © 1998, Nature Magazine, Macmillan Publishers.

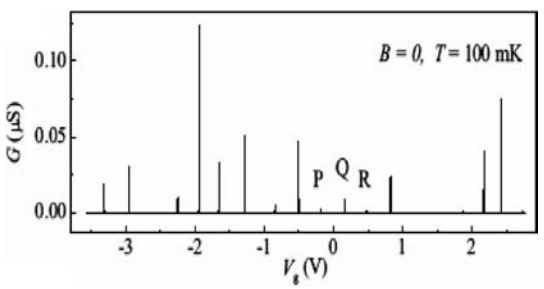

Fig. 4. Sharp spikes in the conductance (G), characteristic of Coulomb blockade and single electron tunneling, is seen in electrical transport through a SWNT as the gate voltage (V_g) is varied. Reprinted with permission from [56], J. Nygard et al., *Appl. Phys. A* 69, 297 **(1999)**. © 1999, Springer-Verlag.

and imperfect screening due to Luttinger liquid behavior (Section 2.1), where it is found (at <5 mK) that an applied gate voltage significantly changes the electronic spectrum through inducing spin flips. The transport measurements, in a magnetic field, can help in the determination of the ground-state spin configuration and a need for a better model than simple Coulomb Blockade is felt. The Zeeman energy splitting ($= g\mu_B B$) was used[60] to determine the gyromagnetic ratio (g) to be $\sim$2.04 indicating the absence of orbital contributions. The ground state of a short SWNT, exhibiting quantum dot like characteristics, was hypothesized[60] to alternate between the $S = 0$ and $S = 1/2$ states. These results are in contrast to those of Tans[59] et al. where it was stated that electrons enter the nanotube with the same spin (with a unique S), at low fields. These observations indicate that studies beyond the single electron picture are imperative to describe the low energy electron transport in SWNTs.

It was also found through scanning probe techniques[61] that semiconducting nanotubes had significant potential fluctuations along the length of the nanotube, more so than in the case of metallic nanotubes. This is equivalent to breaking the nanotube into a series of quantum dots and is particularly insidious to the conductance of semiconducting SWNTs. If the disorder is long-range, the difference in the transport characteristics between semiconducting and metallic tubes could be explained, and lead to much larger mean free paths (>1 μm) in the latter variety.[62]

3. MULTI-WALLED NANOTUBES (MWNT)

MWNTs are composed of coaxial nanotube cylinders, of different helicities, with a typical spacing of $\sim$0.34 nm,[27] which corresponds closely to the inter-layer distance in graphite of 0.335 nm.[21] These adjacent layers are generally non-commensurate (different chiralities) with a negligible inter-layer electronic coupling and could alternate randomly[63, 64] between metallic and semiconducting varieties. The layers, constituting the individual cylinders, are found to close in pairs at the very tip of a MWNT, and the detailed structure of the tips plays an important role, say in the electronic and field emission[65] properties of nanotubes. While there was debate on whether the individual nanotubes close on themselves or the tubes are scrolled, it is currently accepted through the evidence of high resolution electron microscopy studies[66] that the latter i.e., the *Russian doll* model is more likely to be true. Typical MWNT diameters grown by the arc-discharge method are $\sim$20 nm, while CVD grown nanotubes can have much larger diameters of up to 100 nm. (In literature, a wide variety of filamentous/segmented/non-continuous carbon nanostructures are often classified under the category of nanotubes, but which should really be called nanofibers[14]) Larger diameter tubes are found to have a greater density of defects, i.e., vacancies or interstitials.

3.1. Electronic Structure

As MWNTs are composed of several coaxial SWNTs it might be expected that they are not strictly one-dimensional conductors. However, a pseudo-gap was observed[67] in I–V measurements with a power scaling law for the conductance, characteristic of Luttinger liquid (Section 2.1) like behavior. It has been found that the LL parameter g scales as $\sqrt{N}$, where N is the number of tubules screening the charge in the MWNT. It was also determined[68] (see also Section 3.3.1) that the current flow only occurs through the outer most nanotube cylinder (which could also result from the contact geometry with deposited metal electrodes). Consequently, many features peculiar to reduced dimensionality can be studied in MWNTs as well. Also, while the mutual interaction between the adjacent coaxial cylinders might be very small, it cannot be completely neglected, and which makes for a richer band structure[69] in contrast to SWNTs and comparable to graphite (where the inter-plane coupling is $\sim$10 meV). Inter-tube coupling (which depends inversely with the MWNT diameter[70]) can also significantly affect the band structure. For instance, in a two wall nanotube, one metallic and the other semiconducting low energy properties characteristic of metallic tubes predominate while if both the constituent tubes are metallic, a much more complicated situation in terms of band crossings can arise. As an example, it was shown that[71] in a n-wall armchair nanotube n^2 avoided band crossing can occur leading to the formation of pseudo-gaps in the density of states. The consequent strong coupling between the electronic states at the Fermi level (E_F) and the phonon modes may then cause superconductivity.[71] Additionally,[27] strong band structure modifications can also be expected if the constituent undoped nanotubes were of different chiralities. However, in the case of different chiralities (say, arm-chair *and* zig-zag) the total DOS would just be the sum of the individual density of states.

3.2. Transport Characteristics

The electrical conductivity of MWNTs can be modeled to be comparable with that of independent graphene sheets. When the tube diameter (d_t) is smaller than the elastic mean free path (l_e), the one-dimensional ballistic transport predominates, while, if d_t is larger than l_e, the current flow could be described as diffusive/two-dimensional transport. Another quantity of importance[46] is the phase coherence length (l_ϕ) which was determined, through an elegant experiment[68] exploiting the Aharonov-Bohm effect, to be $\sim$250 nm, even larger than the diameter of the MWNT! However, the value of l_ϕ inferred from direct I–V measurements was $\sim$20 nm; the discrepancy could arise from poor Ohmic contacts. Another source of difference could also be due to the quality of the MWNTs; higher temperature growth processes (say, arc-growth) synthesize *cleaner* MWNTs and exhibit metallic temperature dependence,

where the resistance linearly decreases with temperature. Coulomb Blockade effects, which are almost always observed in SWNTs at low temperatures, do not seem to be particularly relevant for MWNTs.

Quantized conductance, corresponding to multiples of G_o ($\frac{2e^2}{h}$) and ballistic transport, was measured,[72] at room temperature, in a single MWNT mounted on a scanning probe microscope (SPM) tip and dipped into liquid mercury metal. While a conductance of $2G_o$ should have been observed in the absence of magnetic fields, it was assumed for the interpretation of the experimental results, that the spin degeneracy was resolved through electron-lattice structure coupling. In yet another experiment, where the MWNT was grown *in situ* on a tungsten contact, for better contact resistance, and probed with a W tip, a conductance of up to 490 G_o (corresponding to a current of 8 mA in a 100 nm diameter MWNT) was observed,[73] characteristic of multi-channel quasi-ballistic transport. Generally, measurements of nanotubes placed on/below metal electrode contacts on substrates suffer from non-reliable Ohmic contacts—a recurring theme in electrical characterization. In measurements, using contacting electrodes patterned through STM lithography, it was shown[74] that at low temperatures (~20 mK) electron interference effects typical of disordered conductors are present in the transport characteristics. A logarithmic decrease of the conductance with temperature followed by a saturation was taken to be the evidence for two-dimensional weak localization[4] effects (Fig. 5) Further evidence of localization phenomena is manifested through the observation of a negative magneto-resistance (MR) and a low value (<20 nm) for the l_ϕ (note that localization effects are important only in the case, $l_\phi < d_t$).[75]

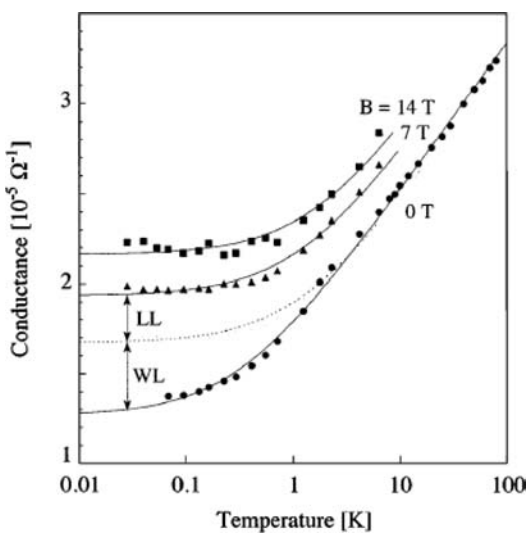

Fig. 5. The electrical conductance as a function of temperature for a MWNT exhibits an initial decrease followed by saturation at low temperatures. Weak localization behavior is manifested at temperatures <60 K, plotted as a function of the magnetic field (B). The presence of disorder is thought to be responsible. Reprinted with permission from [74], L. Langer et al., *Phys. Rev. Lett.* 76, 479 **(1996)**. © 1996, The American Physical Society.

In doped MWNTs, the Fermi energy (E_F) is shifted changing the total number of participating conduction channels. Localization effects have also been observed[76] in B doped MWNTs, along with a negative MR, below ~60 K. The overall temperature dependence of the conductance (G) is then:

(i) an initial linear decrease of G from 300 K–60 K,
(ii) a log (T) variation from 60–1 K, and
(iii) a saturation at low temperature (<1 K).

(It is interesting to note that in disordered graphite at low temperatures, carrier localization leads to a resistance increase (with a typical sheet resistance, R_s of ~100 kΩ) while crystalline graphite is characterized by a metallic R_s of ~1 kΩ).

3.2.1. Magneto-Resistance Measurements

Electron-electron interactions do have to be considered in explaining the magneto-resistance (MR) measurements on nanotubes. A typical MR measurement of a MWNT in a *perpendicular* magnetic field[67] (Schonenberger, 1999) is shown in Figure 6(a) where the fits to the lines are made using one-dimensional weak localization theory and the conductance change (ΔG) $\approx$ ($\frac{2e^2}{h}$)$\frac{l_\phi}{L}$ is used to calculate the phase coherence length (l_ϕ). The strong temperature dependence of the conductance is modeled through $G\alpha T^\delta$, where $\delta < 0.3$ (In SWNTs, δ can be as large as 0.8 due to reduced screening effects). It was noted, with a theoretical basis from the Onsager reciprocity relations,[46] that the two-terminal resistance was symmetric in a magnetic field while the four terminal resistance could be asymmetric. Universal conductance fluctuations (UCF), of magnitude $\frac{e^2}{h}$, characteristic of stochastic, quantum interference effects[77] in the sample have also been observed in MR measurements. While disorder in the nanotube could cause the UCF, it is also likely that chaotic scattering of the electrons, in a nanotube cavity, could also be responsible.

While the weak localization effects monotonically disappear for the case of a perpendicular field, in contrast, a *parallel* magnetic field causes a periodic, ($\Delta B = (\frac{h}{2e})\frac{1}{A}$) modulation of the localization effects which is area (A) dependent—Figure 6(b). In the parallel case, the threading magnetic flux (ϕ) gives rise to an Aharanov-Bohm phase which modifies the boundary conditions transverse to the nanotube. From the Altshuler–Aronov–Spivak (AAS) theory[68] this led to the conclusion that the current in a MWNT only traverses the outermost tubule.

In summary, the wide variety of electrical transport characteristics could be due to the differences in their growth conditions and method of probing/contacts. Consequently, MWNTs display characteristics ranging from localization to metallic behavior at low temperature resulting in either a small or large phase coherence length. The

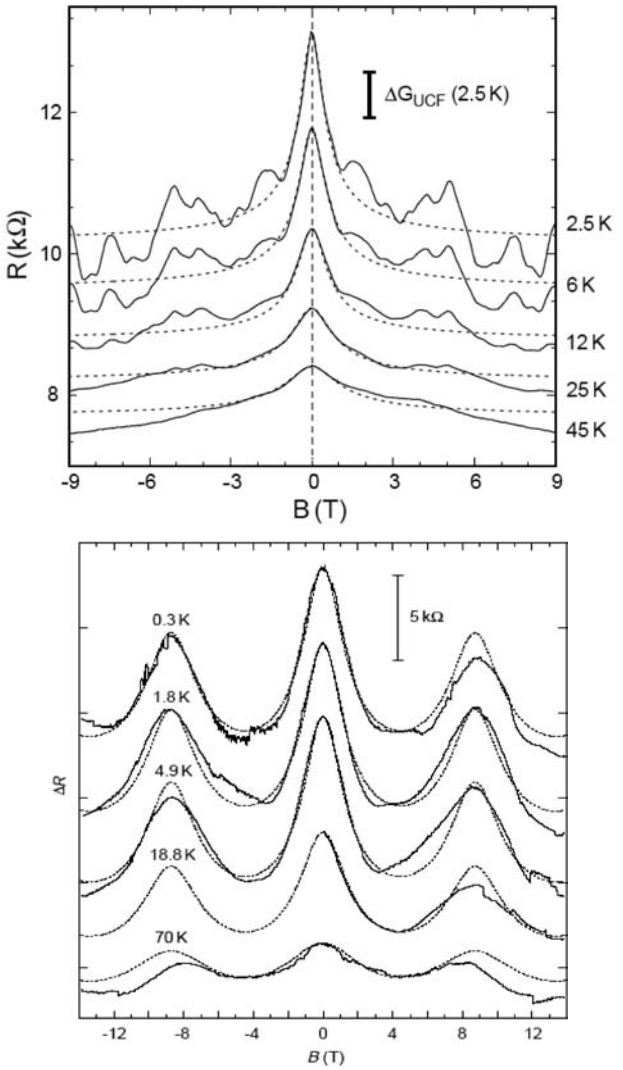

Fig. 6. Negative magneto-resistance (MR) is observed in a MWNT placed *perpendicular* to a magnetic field. Reprinted with permission from [27], L. Forro and C. Schonenberger, Physical properties of Multi-wall Nanotubes, Carbon Nanotubes—Topics in Applied Physics, edited by M. S. Dresselhaus, G. Dresselhaus, and P. Avouris, Springer-Verlag, Heidelberg, **(2001)**. © 2001, Springer-Verlag, Berlin; (b) The magnetoresistance of a MWNT placed *parallel* to a magnetic field exhibits characteristic (h/2e) oscillations. A phase coherence length (l_ϕ) of 200 nm has been inferred. Universal Conductance Fluctuations (UCF) in the resistance are present, e.g., see data at 0.3 K. Reprinted with permission from [68], A. Bachtold et al., *Nature* 397, 673 **(1999)**. © 1999, Nature Magazine, Macmillan Publishers.

non-local interactions manifest in a disordered sample can cause difficulties in the interpretation of even four-terminal measurements.

4. SUPERCONDUCTIVITY

A postulated mechanism of superconductivity in one-dimensional SWNTs involves the reversal of the *normally* repulsive interactions of the Luttinger liquid. This may happen, for instance, when the curvature[78] of CNTs leads

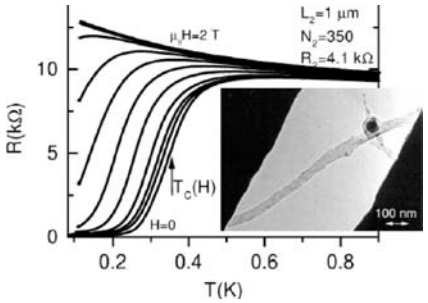

Fig. 7. Observation of superconductivity on SWNT ropes. A T_c of ~0.5 K is inferred. The length (L_2), the number of nanotubes in the bundle of ropes (N_2) and the room temperature resistance (R_2) are indicated on the figure, along with the response to the magnetic field. Reprinted with permission from [80], M. Kociak et al., *Phys. Rev. Lett.* 86, 2416 **(2001)**. © 2001, The American Physical Society.

to the creation of new electron-phonon scattering channels and consequent *attractive* electron phonon interactions[79] can induce superconductivity. It was also proposed that the superconducting transition temperature (T_c) could be enhanced by chemical doping of the nanotubes, by analogy with the higher transition temperatures in alkali doped fullerenes.

A T_c of ~0.55 K was measured[80] (Fig. 7) in ropes of SWNTs connected to non-superconducting metallic (Pt/Au) pads. From the Bardeen–Cooper-Schrieffer (BCS) relations ($\Delta = 1.76 k_B T_c$) a superconducting gap (Δ) of ~85 μeV and a coherence length ($\xi = \sqrt{(\hbar v_F l_{mfp})/\Delta}$) of 300 nm was inferred, for a mean-free path length (l_{mfp}) of ~18 nm and a Fermi velocity (v_F) of $8 \cdot 10^5$ m/s. A higher T_c of 15 K was reported [81] in 04 nm SWNTs embedded in a zeolite matrix, accompanied by the observation of an anisotropic Meissner effect, characteristic to one-dimension. Such an effect is very intriguing in that a strictly one-dimensional system is unstable to any fluctuations and true superconducting behavior can only be observed at $T = 0$ K.

It was also shown that[82] superconductivity could be induced in a metallic nanotube bundle in close proximity with a superconducting electrode (Re/Ta on Au), on a characteristic length scale, bounded by both the phase coherence length (l_ϕ) and the thermal diffusion length (l_T). Induced superconductivity was inferred through the existence of Josephson supercurrents, with a magnitude *exceeding* the theoretically predicted value of $\frac{\pi\Delta}{eR_N}$ (Δ is the superconducting gap, R_N-the normal resistance of the junction). To explain the observation of higher than expected value of the supercurrents, it was hypothesized that the superconducting state in the nanotube could have been stabilized by the macroscopic superconductivity of the contacts. On the other hand, supercurrents were not observed[83] in SWNTs connected to Nb electrodes; however, the transport behavior was seen to be dominated the effect of the contacts, tuned by varying a back-side gate voltage (V_g). The contacts were varied between (i) high (V_g set

to −40 V), and (ii) low transparency ($V_g = 0$ V) to incident electrons. At high interface transparency, characteristics of Andreev reflection (where an incident electron at the contact is converted into a Cooper pair with the concomitant introduction of a reflected hole) were noted. In the tunneling regime, where the contacts are relatively opaque to incident currents, the *I–V* behavior was comparable to SWNT attachment to non-superconducting electrodes. While the above observations do not explicitly take into account electron-electron interactions, it seems necessary to consider Luttinger liquid behavior for explaining very low temperature (40 mK) spectra and superconducting correlations in one-dimension more fully.

5. THERMOELECTRIC PROPERTIES

It has been found recently[84, 85] that dimensional restriction can lead to a much enhanced efficiency over traditionally used bulk thermoelectrics. Nanotubes offer a natural template for exploring the effects of reduced dimensionality towards fabricating the *best* thermoelectric[86] material. However, in the case of intrinsic/undoped SWNTs, due to symmetry considerations, the electron and the hole thermopower (S) contributions exactly cancel out and the Seebeck effect[87] is not exhibited. This can also be formally derived from the Mott-relation, which relates S to the density of states (DOS) at the Fermi level:

$$S = \frac{\pi^2}{3}\frac{k_B^2 T}{e}\frac{d(\mathrm{DOS}(E_\mathrm{F}))}{dE_\mathrm{F}}$$

In a metallic nanotube, the derivative $\frac{d(\mathrm{DOS}(E_\mathrm{F}))}{dE_\mathrm{F}}$ is zero, which implies a zero S. It is also interesting to note that in the case of phonon or electron *ballistic* transport, $S \to 0$. (The heat current, in analogy to an electric current, is $N G_\mathrm{T}\Delta T$, where N is the total number of acoustic modes, the thermal conductance quantum[88] (G_T) is $\frac{\pi^2}{3}\frac{k_\mathrm{B}^2 T}{h}$, and ΔT the temperature difference along the nanotube). Any effects that break electron-hole symmetry, i.e., doping, impurities etc., in the nanotube can however contribute to a thermopower due to a larger DOS (E_F), which is enhanced in low-dimensional nanostructures.

Generally, the efficiency of a material's thermoelectric performance is quantified by a figure of merit (ZT), where T is the temperature of operation, and $Z(=\frac{S^2\sigma}{k})$. A high ZT then, often demands that a set of incompatible criteria have to be simultaneously fulfilled, i.e., a high thermopower/Seebeck coefficient S (which is greatest for insulators), large electronic conductivity σ (indicated by metallicity), and low thermal conductivity k (which consists of both the phonon contribution: k_lattice and an electronic part: $k_\mathrm{electronic}$). Indeed the ideal thermoelectric material has been described[89] as a phonon-glass (low k)-electron crystal (large σ). Artificially fabricated quantum confined structures, say quantum wells, have shown promise[85, 90–92] in this regard by increasing the S through carrier confinement, modulation doping which increases σ and the presence of interfaces which may enhance long wavelength phonon scattering, thus decreasing k_lattice (Note that the $k_\mathrm{electronic}$ is proportional to σ through the Wiedemann-Franz law).[22]

Early measurements[93] of the thermoelectric effects were performed in mats of nanotubes (of both metallic and semiconducting variety) where the breaking of the electron-hole symmetry, for the observed thermopower, was ascribed to inter-nanotube interactions (which again, can enhance the DOS[94]). As mentioned earlier (section 2.1) a pseudo-gap of 0.1 eV can be opened up through these interactions and was confirmed through an increase of the resistivity of the nanotube bundles at low temperature. (It is also possible that weak metallic links between the nanotubes are contributing to the measured S). The thermopower, measured, was proportional to the temperature, with a value of +60 μV/K at 300 K (Fig. 8), and tended to zero at low temperatures (cf., commercially used Bi_2Te_3 thermoelectrics have an S of ∼250 μV/K) The holes, typical of p-doped nanotubes, were the responsible carriers, as the sign of thermopower follows the sign of the dominant carrier. It was also assumed that the E_F is considerably shifted into the valence band. Slightly higher thermopower (S) values of up to 80 μV/K were obtained on measurements[94] on carbon nanotubes, where the Kondo resonance effect (manifested through a resistance minimum at ∼40–300 K, dependent on the catalyst particle) was thought to be a mediating factor. The interaction of the Fe, Co, and Ni nanoparticles, inevitably present during catalytic synthesis, with the electron spins in the nanotubes was hypothesized to be playing a role in enhancing σ, S and the thermoelectric efficiency. To overcome the uncertainties associated with the above measurements, such as inter-nanotube and substrate interactions, experiments were also carried out

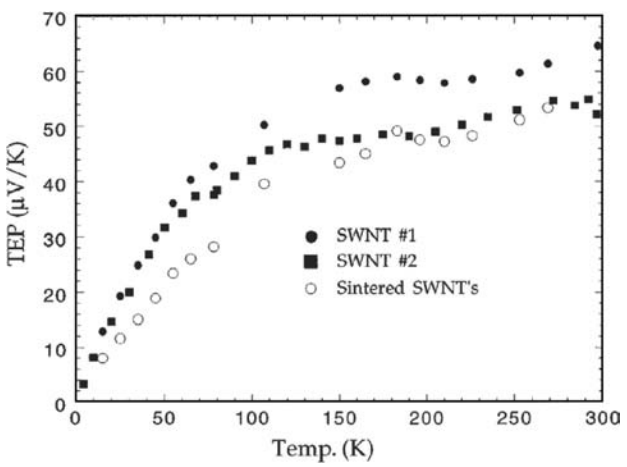

Fig. 8. The variation of the thermopower with temperature for three different SWNT samples Reprinted with permission from [93], J. Hone et al., *Phys. Rev. Lett.* 80, 1042 **(1998)**. © 1998, The American Physical Society.

on individual suspended CNTs.[95,96] In this case a linear variation of the S with temperature was seen along with a two orders of magnitude increase in the measured thermal conductivity over bulk/mat samples. The modulation of the conductance and the thermoelectric power, through an external gate voltage, with a peak S of 260 μV/K at room temperature was also accomplished[97] on individual SWNTs.

It is to be noted, for calculating the thermoelectric efficiency ZT, that there is a wide discrepancy in the measured values of the thermal conductivity, ranging from 20 W/mK in MWNT mats[98] to 3000 W/mK (comparable to the in-plane thermal conductivity of graphite) in suspended nanotubes[96] at room temperature. These numbers are much lower than the theoretically expected value[99] of 6600 W/mK (due to decreased phonon scattering in one-dimension) and correspondingly give a large range of the performance efficiency: ZT at $T = 300$ K ranges between 0.3–3. (It is commonly accepted that a ZT > 1 would compete with existing thermoelectric materials and ZT > 4 would be necessary to simulate technology replacement in devices such as heat pumps and power generators). However, note that in measurements on nanotubes the traditional view of thermal conductivity, as derived from Fourier law of heat conduction, may have to be modified[100] due to the inherent assumptions of diffusive transport. In view of the proposed utility of nanotube composites for thermal management,[101] the investigation of the thermoelectric properties of nanotubes towards application in current generation and heat recovery is one of the exciting directions in nanotube technology. A scientific motivation also arises from the theoretical interpretation that the best thermoelectric[86] is one with a delta function DOS,[102] which is eminently satisfied in the band structure spectrum of nanotubes (see Sections 2.1 and 6).

6. PHOTOCONDUCTIVITY AND LUMINESCENCE

CNTs have a direct band gap and their optical spectra have been interpreted in terms of transitions between free-particle π and π^* bands. The confinement of the electronic states in a one-dimensional system also results in van Hove singularities in the nanotube density of states (DOS) which can be accessed by resonant photons of the appropriate energy (these singularities can occur in both metallic and semiconducting nanotubes).[103] A resonant enhancement due to the divergent nature of the singularities[104] can then be exhibited (Each type of (n_1, n_2) nanotube exhibits a different set of van Hove singularities due to the geometry of wrapping and a different set of electronic transition energies, which can hence be used as a diagnostic technique such as Raman Spectroscopy.[44])

There is a strong anisotropy of optical absorption and emission due to antenna-like interactions[105] (where the size of the nanotubes compares with the wavelength of incident light), and the optical transitions induced by the light parallel to the *long* nanotube axis is orders of magnitude stronger than the intensity of the transitions perpendicular to the axis. The difference between parallel and perpendicular exposure of the nanotubes to light was noted as being similar to that of planar graphite. The selection rules for the photon transitions depend on the exciting light polarization and are derived from group theory.[104] For light polarized parallel to the nanotube axis, only dipole-transitions from the valence band to the conduction band of the same symmetry (labeled as an $E_{n\to n}$ transition, where the E refers to doubly degenerate levels) are allowed. In the case of light polarized perpendicular to the nanotube axis, only the $E_{n\to n\pm1}$ transitions are permitted. Circularly polarized light propagating along the SWNT axis can be used to probe the chirality (which is manifested in terms of the relative intensity of the $E_{n\to n+1}$ and the $E_{n\to n-1}$ transitions). Raman spectroscopy measurements[106] have also been used to measure various sub-band energies and quantitatively determine metal and semiconducting SWNT band energies. The dielectric response ($\varepsilon = \varepsilon_1 + i\varepsilon_2$ of oriented nanotube films have been determined through ellipsometry.[107]

A strong confinement between photo-excited electrons and holes, in low dimensional structures can create strongly bound excitons with an increased binding energy (E_B). A variational approach was used to determine[108] that there is a significant enhancement in the E_B with a power law dependence (Fig. 9) on the nanotube radius (r) following $r^{-0.6}$. It was also concluded that the optical transition energy can be lowered by as much as 40% and excitons provide a strong correction to the CNT electronic energies. Experimental evidence for excitonic states have been

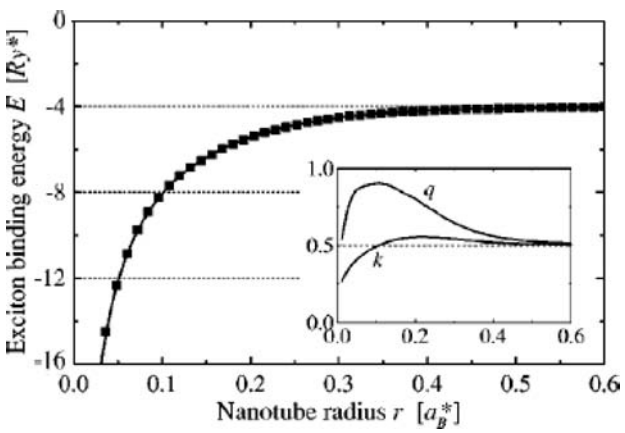

Fig. 9. The variation of the exciting binding energy (E) as a function of the nanotube radius. A significant enhancement factor up to a factor of ten, due to confined excitons in one-dimension, is predicted for small diameter semiconducting nanotubes. The inset shows the spatial extent of the exciton wave function (k and q refer to the variational parameters used and are related to the exciton radius). Reprinted with permission from [108], T. G. Pedersen, *Phys. Rev. B* 67, 073401 **(2003)**. © 2003, The American Physical Society.

obtained through laser excitation.[109, 110] The observation[109] of an additional peak in the absorption spectra (∼190 meV) above the expected E_{22} van Hove transition was correlated to excitons and exciton-phonon coupling. The width of the peak was related to exciton dispersion effects. In the latter experiment with pump-probe spectroscopy,[110] a Mott transition indicating a highly correlated exciton gas was indicated.

In examining the effects of illumination, excitations intrinsic to the nanotube should be carefully distinguished from photodesorption effects. For example, it has been shown[111] that UV light (∼254 nm) can desorb oxygen molecules bound on nanotube surfaces at light intensities as small as 20 μW/cm^2. As oxygen functions as an electron acceptor/hole donor in nanotubes (see Section 2.2), its removal lowers the hole concentration in p-type SWNTs and reduces the electrical conductivity. It has been suggested that such a molecular desorption process could also be mediated through photo-excited plasmons. The hot electrons/holes from the plasmon de-excitations attach on to the adsorbed molecules and induce desorption.

Fluorescence, with a quantum yield of 10^{-3} and a lifetime of 2 ns, between singlet excitonic levels has been obtained from isolated SWNTs.[112] However, photoluminescence (PL) was not observed[112] for SWNT bundles, possibly due to rapid charge transfer in between the nanotubes, which allows rapid relaxation of the photo-excited carriers. To guard against such effects and measure the *true* response both (1) photoconductivity[109, 113] and (2) electroluminescence (EL)[114, 115] experiments were carried out on *single* CNT constituted FETs with an oxide capping layer.[113]

To measure the photoconductivity, a nanotube transistor was nominally operated[113] in the OFF state to minimize the dark current background and noise level. A linearly polarized, CW Ti: Sapphire laser that is continuously tunable between 780 nm (1.59 eV) and 980 nm (1.27 eV), with a power density of 1 kW/μm^2 was shone on the nanotube. A peak in the photocurrent corresponding to a E_{22} transition was observed as the incident energy was varied (Fig. 10(a)). The photocurrent depends strongly on the light polarization direction, with a maximum when the light is polarized in the direction of the nanotube axis (Fig. 10(b)) and a minimum in the perpendicular direction. A quantum efficiency of 10% was inferred through finite element analysis.

A CNT FET with thin Schottky barriers at the Source and Drain electrodes (Fig. 11(a)) can allow the simultaneous injection of electrons and holes which permits the construction of a light-emitting device *without* the necessity of doping (or creating a p-n junction). This principle was used[114] in an ambipolar nanotube FET, where the gate was biased exactly in between the source and the drain i.e., the source electrode was grounded (i.e., $V_s = 0$), the gate (V_g) was placed at +5V and the drain (V_d) at +10 V. This creates electric fields of opposite signs at the source and drain

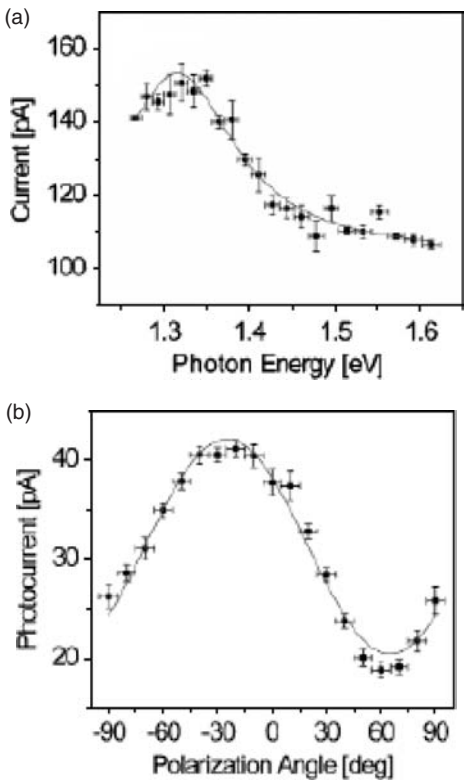

Fig. 10. (a) Light induced photocurrents in nanotubes, as a function of incident photon energy. Both the experimental data and the Lorentzian fits are shown (b) The light emission varies with the angle of polarization, with a maximum when the light is polarized in the direction of the nanotube axis. The photocurrent for parallel excitation is twice greater than that for perpendicular excitation. As a function of the polarization angle. Reprinted with permission from [113], M. Freitag et al., *Nanolett.* 3, 1067 **(2003)**. © 2003, The American Chemical Society.

electrodes, and there is an equal injection of electrons (n-type modulation) from one end and holes (p-modulation) from the other. This is also *equivalent* to creating a forward biased p-n junction. The band diagram is shown in Figure 11(b) as a function of nanotube length. It was seen that the nanotube operated as a source of linearly polarized infra-red emission (<1500 nm), with a peak intensity at $V_g = V_D/2$ (Fig. 11(c)). When this bias condition was not satisfied, i.e., with unipolar operation no IR emission was observed precluding thermal effects from contributing to the observed emission. The EL also depends on the length of the nanotube, through the interplay of the phonon scattering time and the carrier transit time. For example, in short (∼0.5 μm) CNTs the acoustic phonon scattering (of time scale ∼0.4 ps) is too slow and only the optical phonons (0.02 ps) contribute to carrier thermalization during the transit time of ∼0.6 ps. On the other hand, in longer CNTs (>10 μm, say) the transit time is ∼60 ps and complete carrier relaxation is obtained. Consequently, the emission spectra are narrower from shorter nanotubes. These effects are especially important in high electric field transport,[116] where phonon assisted radiative recombination can play a major role in the overall luminescence.

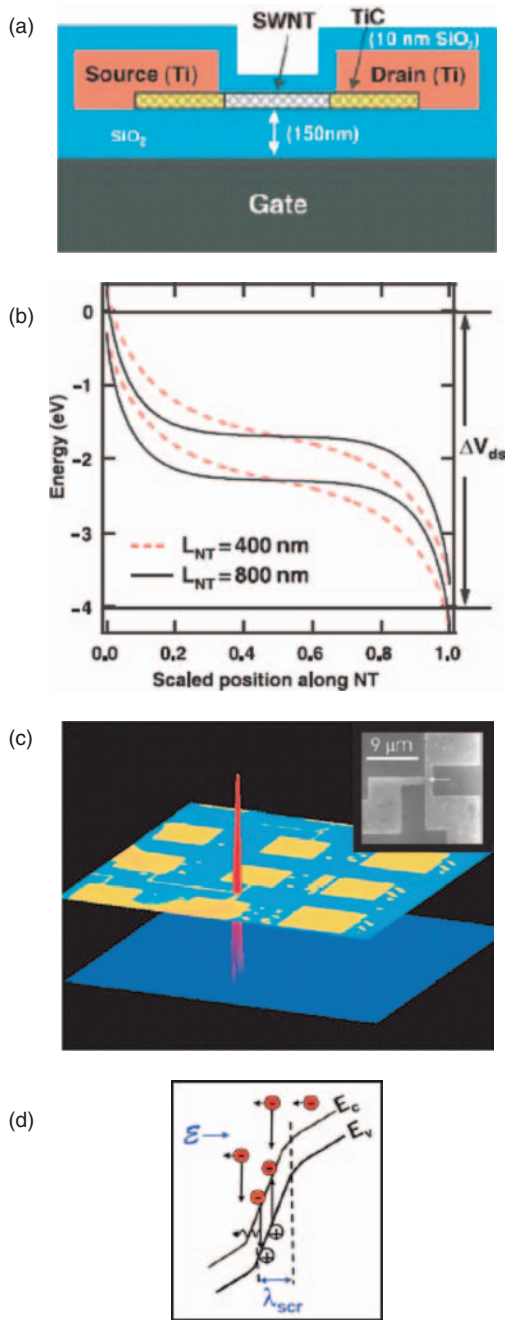

Fig. 11. (a) A typical device topology, comprising an *ambipolar* SWNT, for measurement of the optical properties of nanotubes, (b) The band structure of the device is comprised of two back-to-back Schottky diodes, through which electrons and holes are simultaneously injected for recombination and optical emission. Note that the band curvature is more marked for a shorter tube ($L_{NT} = 400$ nm) compared to a larger tube ($L_{NT} = 800$ nm). This has implications in whether a particular SWNT is optimized for light emission/photovoltage generation (see text) (c) the observed optical emission is localized as illustrated in the infra-red image, Reprinted with permission from [114], J. A. Misewich et al., *Science* 300, 783 **(2003)**. (d) A larger intensity of light emission can be obtained by inducing electroluminescence in suspended nanotubes. The abrupt junction between a contact and a suspended SWNT causes hot electron formation and subsequent radiative exciton decay. Reprinted with permission from [115], J. Chen et al., *Science* 310, 1171 **(2005)**. © 2005, Science Magazine.

It is interesting to compare[113] the CNT band structure needed for photovoltage generation and operation as a light emitting device for ambipolar operation. In both cases, the carrier tunneling through the Schottky barriers are important. In the case of *photovoltage* generation, the barrier should be *opaque* to electrons and holes and a large electric field at the center would help to separate the carriers. For *light emission* however, a relatively *transparent* Schottky barrier is desirable for easy carrier injection and flat bands at the center promote their radiative recombination. The curvature of the bands can be regulated by the gate oxide thickness, where a thinner gate oxide can promote charge tunneling through the barriers. It was also seen that the point of emission (i.e., the ambipolar domain)[117] could be tuned along the length of the nanotube by varying the gate voltages. The relative values of the contact and nanotube resistance determine the range of voltages and the intensity of emission is correlated with the magnitude of the current.

In the experiments described, the SWNTs were supported in close proximity to the substrate with the possibility of non-radiative recombination of the injected electrons and holes. A new mechanism of EL, with unipolar conduction at lower drain bias, was reported[115] in suspended ($\sim$2 μm above the substrate) nanotubes, where high local electric fields at the suspension interface were found to enhance the emission efficiency by almost a factor of 1000 (10^{-3} vs. 10^{-6} in ambipolar devices).[116] The efficiency was exponentially proportional to the ratio of the applied electric field to the interface electric field. At the point of suspension, there is a dramatic bending of the CNT bands, due to a decreased capacitive coupling to the substrate, with a concomitant high local electric field (Fig. 11(d)). Consequently, hot carriers can be generated through impact excitation which can create radiatively decaying excitons (provided that the optical phonon scattering can be avoided). A threshold electrical field of $1.5\frac{E_g}{\lambda_{ph}}$ is needed, which was estimated to be $\sim$0.6 MV/cm (assuming an energy gap E_g of 0.6 eV and an optical phonon scattering length, λ_{ph}, of $\sim$15 nm). The one-dimensional character of SWNTs is helpful in increasing the exciton binding energy (E_B) while also being amenable to observe exciton dynamics and recombination. As an example, it was observed[115] that the formation of the E_{22} excitons was due to annihilation of two E_{11} excitons.

7. NOVEL ELECTRONIC FUNCTIONALITY *via* BRANCHED CARBON NANOTUBES

From the above discussion, we note that the electrical properties[118] of both SWNTs[55] and MWNTs have been relatively well explored. While SWNTs can be described as quantum wires due to the ballistic nature of electron transport,[55] the transport in MWNTs is found to be diffusive/quasi-ballistic.[57, 119] Quantum dots can also be formed in both SWNTs[54] and MWNTs[57] and the Coulomb

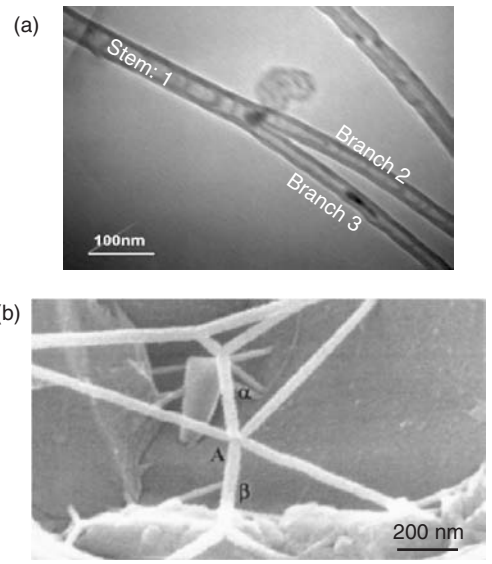

Fig. 12. (a) The Carbon Nanotube (CNT) Y-junction morphology can be used as a novel platform for an integrated electronics, where the gate (say, stem) can be an integral part of the structure for measuring transport properties. Reprinted with permission from [121], P. R. Bandaru et al., *Nat. Mater.* 4, 663 (**2005**). © 2005, Nature Magazine; (b) A more complex three-dimensional CNT network, including Y-, T-, and X-junctions, produced through CVD synthesis.[208] The existence of such negative curvature fullerene based units,[209] and branching in nanotubes necessitates the presence of topological defects—in the form of pentagons, heptagons, and octagons—at the junction regions for maintaining a low energy sp^2 configuration.[210] These *intrinsic* defects are natural scattering centers that could affect the electrical transport characteristics of a nanotube. Reprinted with permission from [122], J.-M. Ting and C.-C. Chang, *Appl. Phys. Lett.* 80, 324 (**2002**). © 2002, American Institute of Physics.

blockade and the quantization of the electron states can be used to fabricate single-electron transistors.[35] While extremely important in elucidating fundamental properties, the above experiments have used external electrodes, made through conventional lithographic processes to contact the nanotubes and do not represent truly nanoelectronic circuits. Additionally, the well known MOSFET architecture is used, where the nanotube serves as the channel between the electrodes (Source and Drain), and a SiO_2/Si based gate modulates the channel conductance. In other demonstrations, cumbersome Atomic Force Microscope (AFM) manipulations[120] of nanotube properties have been utilized.

It would, therefore, be attractive to propose new types of nanoelectronic elements, to harness new functionalities, peculiar to carbon nanotubes. Such novel functionalities can be found for example in CNT morphologies such as Y-junctions[121] (Fig. 12) and even more complex networks,[122] incorporating T- and X-junctions (Fig. 12(b)). (Note that these are *naturally formed* CNT forms and *distinct* from crossed nanotube junctions,[32] where metallic and/or semiconducting nanotubes have to be individually assembled through Atomic Force Microscope manipulations). With Y-junctions as an example, one can envision a more ambitious scheme and circuit topology—where both interconnect and circuit elements are all based on nanotubes, realizing true nanoelectronics. Nanotube based interconnect does not suffer from the problems of electromigration that plague copper based lines, due to the strong carbon–carbon bonds, and can support higher current densities[123] ($\sim$10 μA/nm^2 or 10^9 A/cm^2 vs. 10 nA/nm^2 or 10^6 A/cm^2 for noble metals such as Ag). Additionally, the large thermal conductivity[96] ($\sim$3000 W/mK at 300 K), up to an order of magnitude higher than copper, could help alleviate the problem of heat dissipation in ever shrinking devices. Developing nanotube based devices, besides miniaturization and lower power consumption, will also allow us to exploit the features of inherently quantum mechanical systems, such as ballistic transport and low switching voltages[124] ($\sim k_B T/e$). In this section, we report on the study of the electrical properties of novel CNT morphologies, with Y-junctions as a prime example.

7.1. Electrical Phenomena in Novel Carbon Nanotube Morphologies

Branched nanotubes with T-, Y-, L- and more complex junctions, were initially observed in arc-discharge produced nanotubes.[125] Earlier work on individual Y-junctions in a nano-channel alumina template[126] resulted in the observation of non-linear I–V (Fig. 13) characteristics at room temperature through Ohmic contact[127] and tunneling conductance[128] measurements and has opened up a vista of possibilities. While the current theoretical explanations of the observed electrical behavior in Y-junctions are based on SWNT Y-junctions, the experimental demonstrations were made on MWNTs,[127, 128] which are easier to experimentally manipulate compared to SWNTs. In *straight* MWNTs, it has been shown that electronic conduction mostly occurs through the outermost wall,[68] (Section 3.3.1) and interlayer charge transport in a MWNT is dominated by thermally excited carriers.[129] While the outer wall dominates in the low-bias regime (<50 mV), at higher bias many shells can contribute to the conductance with an

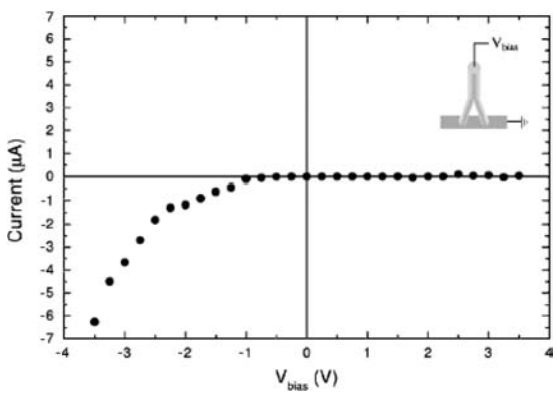

Fig. 13. Diode behavior was observed through the measurement of a Y-junction, using the configuration shown in the inset. A reduction/change in the band gap from a smaller diameter branch to a larger diameter stem was posited to be the reason. Reprinted with permission from [127], C. Papadapoulos et al., *Phys. Rev. Lett.* 85, 3476 (**2000**). © 2000, The American Physical Society.

average current carrying capacity of 12 μA/shell at room temperature.[123] In contrast to SWNTs with μm coherence lengths, the transport in MWNTs is quasi-ballistic[57] with mean free paths <100 nm. Based on the above survey of properties in *straight* MWNTs, it would be reasonable to conclude that non-coherent electronic transport dominates the Y-junctions and other branched morphologies.

7.2. Electron Momentum Engineering in Y-Junctions for More Efficient Electronic Devices

The basic functionality is derived from an electron-wave Y-branch switch[130] (YBS) where a refractive index change of either branch through electric field modulation can affect switching. This device, demonstrated in the GaAs/AlGaAs[131] and InP/InGaAs[132, 133] based two-dimensional electron gas (2-DEG) system, relies on ballistic transport and is useful for low power, ultra-fast (THz) signal processing. It was derived theoretically[124] and proven experimentally[134] that based on the ballistic nature of the electron transport, non-linear and diode-like *I–V* characteristics were possible. These devices based on III–V materials, while providing proof of concept, were fabricated through conventional lithography. It was also shown in 2-DEG geometries[135] with artificially constructed defects/barriers, that the defect topology can affect the electron momentum and guide the current to a pre-determined spatial location independent of input current direction. This type of rectification involves a new principle of *electron momentum engineering* in contrast to the well known *band engineering*. Nanotubes provide a more natural avenue to explore such behavior. It was theoretically postulated[136] that switching and rectification could be observed in symmetric (i.e., with no change in chirality from stem to branch) Y- junction SWNTs, assuming quantum conductivity of electrons, where the rectification could be determined[137] by the:

(i) formation of a quantum dot/asymmetric scattering center[135] at the location of the Y-junction,

(ii) finite length of the stem and branches connected to metallic leads,

(iii) asymmetry of the bias applied/the potential profile[138] across the nanotube, and

(iv) strength of the nanotube-metal lead interactions.

These criteria have been debated upon[139] in relation to whether the non-linear behavior is *intrinsic* to the Y-junction or is due to the metal contacts. Currently, the influence of metal contacts and Schottky barrier formation on nanotube properties[140] and rectification is a very active area of research.

7.3. New Physical Principles and Potential Applications

As an example of novel functionality at the nanoscale, the Y-junctions represent one of the first attempts in realizing a nanoelectronic device from CNTs alone. The motivation for use of new CNT morphologies, in addition to the miniaturization of electronic circuits, is the possibility of new devices and technologies through new physical principles. At the nanometer scale the dimensions of the device are comparable to electron wavelength (λ_F) and electron travel/current must be considered in terms of wave propagation,[141] analogous to the propagation of light down a optical fiber. Wave phenomena, such as interference and phase shifting, can now be used to construct new types of devices. For example, constructive and destructive interferences can be used to cause transmission and reflection of current leading to switching and transistor like applications with added advantage of very low power dissipation. Novel applications, have been proposed theoretically[142–144] for ballistic nano-junctions, of which the Y-junction is only one example. They include:

(a) Switching and Transistor Applications. In a basic Y-junction switch, an electric field can direct electrons into either of two branches, while the other branch is cut off.[124] It has been shown, in computer simulations,[130] that a sufficient lateral field for electron deflection is created by applying a very small voltage of the order of milli-Volts. The specific advantage of a Y-junction switch is that it does not need single-mode electron waveguides for its operation and can operate over a wide range of electron velocities and energies, the reason being that the electrons are not stopped by a barrier but are only deflected. An *operational advantage* over a conventional FET is that the current is switched between two outputs rather than completely turned on/off,[145] leading to higher efficiency of operation.

An electrical asymmetry can also be induced through structural or chemical means across the two branches in a nanostructured junction. The Y-junction region, for instance, can possess a positive charge[136] due to two reasons, *viz.,* the presence of: (1) topological defects,[146] due to the formation of non-hexagonal polygons (e.g., pentagon-heptagon pairs/Stone-Wales defects) at the junction to satisfy the local bond order,[147] where delocalization of the electrons over an extended area leads to a net positive charge, and (2) catalyst particles, which are inevitably present through synthesis.[13, 148] This positive charge and the induced asymmetry is analogous to a "gating" action that could be responsible for rectification/transistor like behavior. While the presence of defects at the junction seems to assist switching, there is also a possibility[136] that such defects may not be needed. Additional studies will elucidate on this aspect, but such an observation is significant in that a three-dimensional array of Y-junction devices based on CNTs would be much easier to fabricate if a particle is not always required at the junction region. The switching voltage (ΔV_s) is proportional to the interaction time between the electron and the scatterer, through the Heisenberg uncertainty relation: $e\Delta V_s \approx \frac{\hbar v_F}{L_i}$,

where v_F is the Fermi velocity and L_i is the interaction length. It is then seen from the above expressions, that both switching efficiency and power consumption is minimized when a nano-sized scattering mechanism is operative as in the Y-junctions.[145] It is also possible to nano-engineer Y-junctions through optimized growth sequences and *in situ* manipulation[149] of the scattering centers can be used to vary *individual* device characteristics.

(b) Rectification and Logic Function. It is possible to design logic circuitry, based on electron waveguiding in Y-junction nanotubes, to perform operations similar to and exceeding the performance of conventional electronic devices.[145] When finite voltages are applied to the left and the right branches of a Y-junction, in a push-pull fashion (i.e., $V_{left} = -V_{right}$ or *vice versa*), the voltage output at the stem would have the same sign as the terminal with the lower voltage.

This dependence follows from the principle of continuity of electro-chemical potential ($\mu = -eV$) in electron transport through a Y-junction and forms the basis for the realization of an AND logic gate, i.e., when either of the branch voltages is negative (say, corresponding to a logic state of 0), the voltage at the stem is negative and positive voltage (logic state of 1) at the stem is obtained only when both the branches are at positive biases.

A change of μ is also not completely balanced out due to the scattering at the junction, and results in nonlinear interaction of the currents from the left and the right sides.[134] To compensate, the resultant center branch voltage (V_S) is always negative and varies parabolically (as V^2) with the applied voltage.[142]

(c) Harmonic Generation/Frequency Mixing. The nonlinear interaction of the currents and the V^2 dependence of the output voltage at the junction region also suggest the possibility of higher frequency/harmonic generation. When an AC signal of frequency ω, $V_{L-R} = A\cos[\omega t]$, is applied between the left (L) and right (R) branches of the Y-junction, the output signal from the stem (V_S) would be of the form:

$$V_S = a + b\cos[2\omega t] + c\cos[4\omega t],$$

where a, b, and c are constants.

The Y-junction can then be used for second and higher harmonic generation or for frequency mixing.[132] The second harmonic (2ω) output is orthogonal to the input voltage and can be easily separated out. These devices can also be used for an ultra-sensitive power meter, as the output is linearly proportional to V^2 to very small values of V. A planar CNT Y-junction, with contacts present only at the terminals, suffers from less parasitic effects (see Section 8.1.3) than a vertical transistor structure and high frequency operation, up to 50 GHz at room temperature,[150] is possible. It can be seen from the brief discussion above that CNT based Y-junction technology could be the forerunner of a new paradigm in nanoelectronics.

7.4. Electrical Transport Measurements

The Y-junction nanotubes, for the electrical transport measurements, were grown[148] on bare quartz or SiO_2/Si substrates through thermal Chemical Vapor Deposition (CVD). The ratio of the Ti-precursor gas and the feedstock gases can be adjusted to determine the *growth of the side-branches at specific positions*. The Y-junction formation has also been found to be sensitive to temperature, time of growth, and catalyst concentration. The growth of nanotube morphologies essentially seems to be a non-equilibrium phenomenon and various other methods have also been found to be successful in proliferating branches, i.e., through a sudden reduction of temperature during a normal tip growth process,[13] where over-saturation by the carbon feedstock gas causes a surface energy driven splitting of the catalyst particle and branch nucleation. Other catalyst particles, such as Ca and Si, have also been found to nucleate side branches.[126] The location of the junction is in any case a point of structural variation[122] the control of which determines the formation of Y-junctions and their electrical properties.

The samples for electrical measurements,[27, 129] were prepared by suspending nanotube Y-junctions (Fig. 14(a)), made through CVD, in isopropanol and depositing them on a SiO_2/Si substrate with patterned Au pads. Y-junctions, in proximity to the Au contact pads, were then located at low voltages (<5 kV) using a Scanning Electron Microscope (SEM) equipped with a Focused Ion Beam (FIB). The ion-beam in the FIB-SEM was used to deposit Pt which connects the Y-junction terminals to the contact pads.

By grounding each branch of the Y-junction successively, the inter- and intra-branch resistances were probed. The characterizations of the capacitive and inductive components of the impedance also give further insight into their physical origins and nanotube structure. The nonlinear characteristics of the Y-junctions, when probed in a three-terminal configuration, are shown in Figure 14(b).

The possibility of using the CNT Y-junctions for *switching applications* as an electrical inverter analogous to earlier[130, 133, 134] Y-switch studies in 2-dimensional electron gases was explored. In this measurement, a DC voltage was applied on one branch of the Y-junction while the current through the other two-branches was probed under a small AC bias voltage of 0.1 V. As the DC bias voltage is increased, at a certain point the Y-junction goes from nominally conducting to a "pinched-off" state. This switching behavior was observed for all the three-branches of the Y-junction, at different DC bias voltages. The absolute value of the voltage at which the channel is pinched off is similar for two branches (~2 V, as seen in Fig. 15(a)), and is different for the third stem branch (~4.6 V, as in Fig. 15(b)). The switching behavior was seen over a wide range of frequencies, the upper limit of 42 kHz, being set by the capacitive response of the Y-junction when the DC current tended to zero.

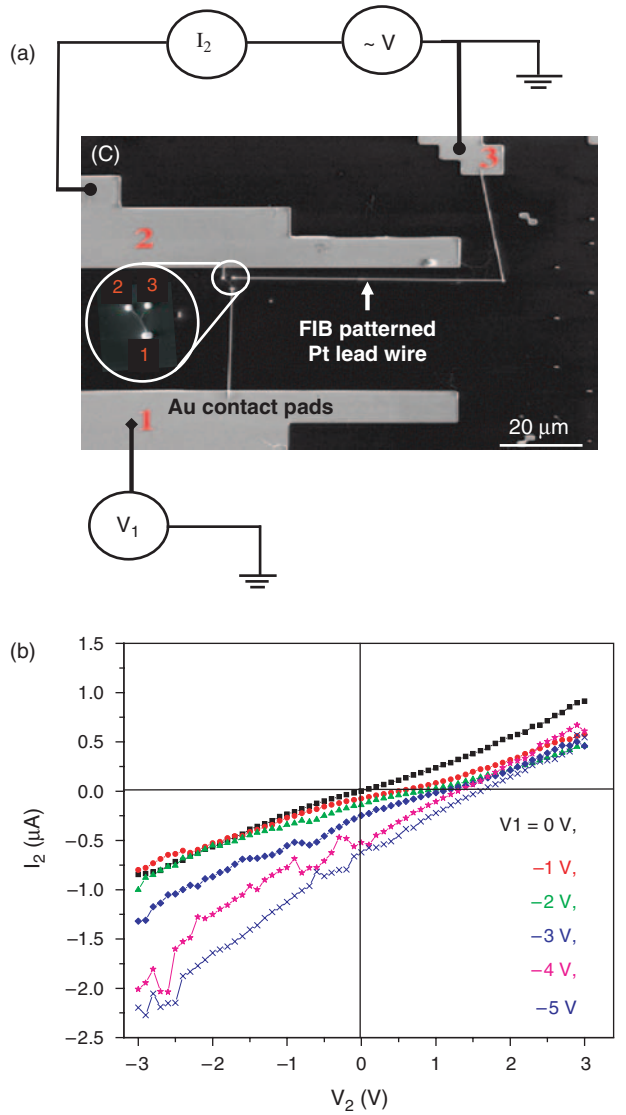

Fig. 14. (a) A SEM micrograph of the overall circuit arrangement used in the measurement of the electrical characteristics, with Au contact pads and a FIB patterned Pt wire contacting the Au pads and the Y-junction. Shown in the figure is an configuration where a control DC voltage is applied on the stem (terminal 1) of the Y-junction, and the current flow through the other two branches in response to a constant AC bias voltage (~V) is monitored. Similarly, control voltages can be applied on branches 2 and 3, for characterizing the Y-junction in detail, (b) Current–Voltage curves for the Y-junction, where the gating action of the *stem* voltage and the asymmetric response[136] is to be noted. Reprinted with permission from [121], P. R. Bandaru et al., *Nat. Mater.* 4, 663 **(2005)**. © 2005, Nature Magazine.

In these experiments, if it is assumed that the Ohmic resistance for all the three contacts is identical, it is possible to identify the individual branch's transport characteristics. (It was not possible to determine all the four impedances: Z_1, Z_2, Z_3 and the contact resistance with 3-terminal measurements). A more in-depth analysis of the contributing factors to the electrical conductivity of a Y-junction is thus possible, e.g., an increased resistance R_1 could result from the presence of a catalyst particle in the stem-section.

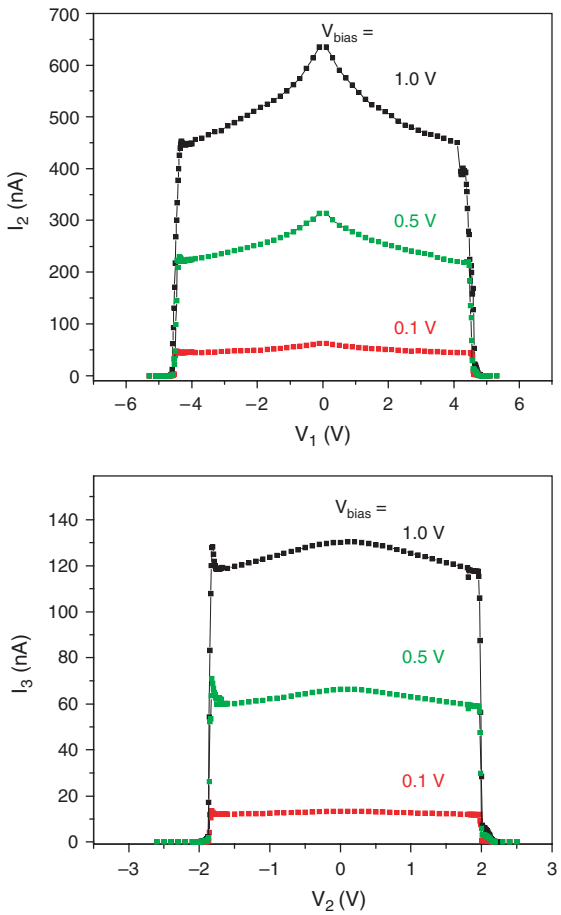

Fig. 15. An abrupt modulation of the electrical current through two branches of the Y-junction is seen on varying the voltage on the third branch. The voltage, at which the switching action occurs, on the stem (1 in Fig. 12(a)) (A) is ~4.6 V, while the turn-off voltages on the two branches (2 and 3 in Fig. 12(a)), as in (B), are similar, at ~2 V. Such a response has been observed up to 40 kHz. Reprinted with permission from [121], P. R. Bandaru et al., *Nat. Mater.* 4, 663 **(2005)**. © 2005, Nature Magazine.

Preliminary evidence of AND (cf., (b) in Section 7.3) logic gate behavior (Fig. 16) was also observed. The logic characteristics are not perfect, however, due possibly to imperfections[151] of the nanostructure and it would be very interesting to, determine the exact conditions for and, demonstrate ideal logic gate characteristics.

The detailed nature of the electrical switching behavior is *not understood* at present. The presence of catalyst nano-particles (Fig. 12(a)) in the conduction paths could blockade current flow, and their charging could account for the abrupt drop-off of the current. The exact magnitude of the switching voltage would then be related to the exact size of the nanoparticle, which suggests the possibility of nano-engineering the Y-junction to get a variety of switching behaviors. An alternative possibility is that there is inter-mixing of the currents in the Y-junction, where the electron transmission is abruptly cut off due to the compensation of currents, for example, the current through branches 2 and 3 is cancelled by current leakage through

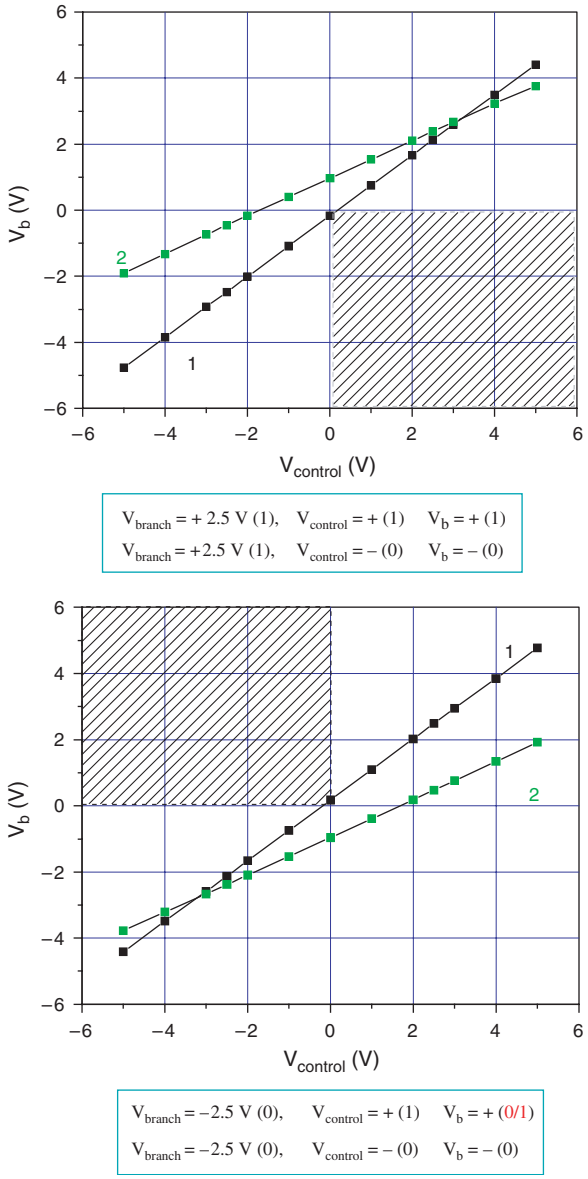

Fig. 16. The carbon nanotube Y-junction can be used as an AND logic gate (see text for details). A constant voltage, (positive in (a) and negative in (b), is applied on one branch (V_{branch}), and the voltage monitored across the second branch (V_b), while a control DC voltage ($V_{control}$) is swept across the third branch of the Y-junction. The two lines (green and black) refer to the possible permutations of the voltages applied on the two branches (2 and 3 in Fig. 12(a)). Reprinted with permission from [121], P. R. Bandaru et al., *Nat. Mater.* 4, 663 **(2005)**. © 2005, Nature Magazine.

stem 1 (cf., Fig. 12(a)). The geometry and defects could also be responsible. Further research is needed to clarify the exact mechanisms in these interesting phenomena.

8. APPLICATIONS OF THE ELECTRICAL CHARACTERISTICS OF NANOTUBES

Richard Smalley, one of the pioneers of nano-carbon related research, was said to have remarked, "These nanotubes are *so* beautiful that they *must* be useful for something." In keeping with this pronouncement, a wide variety of applications are being extensively researched. Although much of this research is still in the university/industrial laboratory a strong foundation is being built for future deployment and heralds the era of carbon nanotube based nanotechnology. A few such applications, by no means exhaustive, are detailed below:

8.1. CNT Electronics

8.1.1. Interconnect Applications

In state-of-the art copper interconnect, used in the microelectronics industry, the scattering lengths are of the order of a few nanometers resulting in large resistances which impose limitations in power dissipation and operating speeds. As an example, it is seen that when[152] the lateral dimensions of copper lines fall below 100 nm, surface and grain boundary scattering cause a significant increase in the resistivity, e.g., in 50 nm × 50 nm copper traces, the resistivity was approximately twice the bulk value. This sets the stage for the possible uses of nanotubes for interconnect applications in ever-shrinking devices. In CNTs ballistic transport (Section 2.3) together with large carrier mobilities allows for a large carrier mean free paths (l_{mfp}) > 1 μm. The origin of this reduced scattering is related to the reduced phase space for phonon scattering in lower dimensional structures. Additional advantages of using nanotubes include a three orders of magnitude increased current density (10^9 A/cm^2 vs. 10^6 A/cm^2 for Ag) and immunity to electromigration (due to the strong C–C bonds).

Practically, however, SWNTs typically have a resistance of several kΩ (Section 2.3), even excluding the contacts, and it was calculated (Section 8.1.3) that their low frequency behavior was dominated by the RC time constant. Additionally, the kinetic inductance (L_K) due to electron movement, could be a factor of 1000 higher than the magnetic inductance (L_M), and dominate the high frequency behavior. These limiting factors are a barrier for the use of nanotubes. An obvious way of extending the speed is to increase the number of current modes that are transmitted through the nanotube. However, this is limited by the diameter and the band structure. Perhaps, then, by comparing equivalent areas of parallel connected nanotube bundles with copper interconnect one can arrive at a better comparison of the efficacy of nanotubes[33] (A copper line width of 50 nm and a height of 100 nm corresponds to a resistance of ~10 Ω/μm and L_M of 1 pH/μm, and is equivalent to approximately thousand nanotubes connected in parallel). Assuming negligible interactions between the constituent wires, the resistance (R) of a CNT of length (L) with a mean free path (l_{mfp}) as a function of the applied voltage (V) is given by:

$$R = \frac{h}{4e^2}\left[1 + \frac{L}{l_{mfp}}\right] \qquad \text{—Low electric field}$$

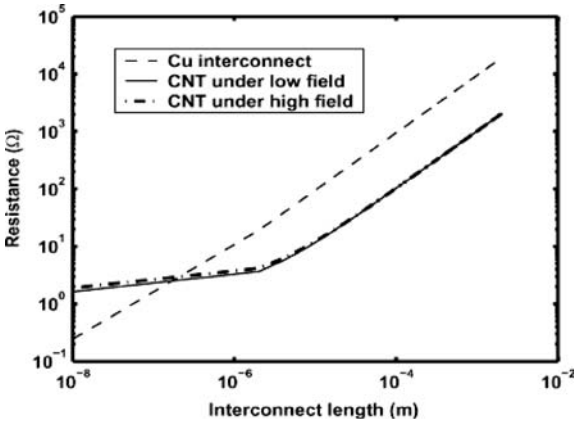

Fig. 17. A comparison of the resistance of *conventional* copper interconnect with parallel metallic SWNTs, of the same dimension, illustrates the greater utility of the latter for interconnect lengths larger than 1 μm. Reprinted with permission from [33], S. Salahuddin et al., *IEEE Trans. Elec. Dev.* 52, 1734 **(2005)**. © 2005, IEEE.

$$R = \frac{h}{4e^2}\left[1 + L\left(\frac{1}{l_{\mathrm{mfp}}} + \frac{1}{0.16L/V + L_{\mathrm{hp}}}\right)\right]$$

—High electric field

While only acoustic phonons are effective for scattering at low fields, optical phonons (with mean energies of ~0.1–0.2 eV) must be considered along with the mean length which the electrons have to traverse for optical phonon excitation ($= 0.16\ L/V + L_{\mathrm{hp}}$). The comparison of the equivalent resistance as a function of interconnect length for nanotubes and copper interconnect is shown[33] in Figure 17. The conclusion is that CNTs can outperform copper interconnect if they could be connected in parallel for lengths larger than 1 μm. The current carrying capacity (of 10^9 A/cm^2) is intrinsically a big advantage corresponding to copper lines as electromigration problems begin to set in Ref. [153] at $\sim 10^6$ A/cm^2. Consequently, in high power applications CNTs are desirable and could make a mark in *long* interconnect due to their high current drive capabilities.

8.1.2. Will Nanotubes Make for a Better Field Effect Transistor?

CNTs have been widely tested and are contemplated for transistor/switching applications in advanced electronics. The device topologies mainly incorporate:
(1) Adaptation to the conventional silicon based MOSFET (Metal Oxide Semiconductor Field Effect Transistor) architecture, where the nanotube serves as the channel.
(2) Novel morphologies, such as Y- and T-junctions which possess an intrinsic functionality in that the gate can be fabricated as a part of the device.[121]

As remarked earlier, the band dispersion for electrons and holes is similar for SWNTs. This has the important implication that devices using p- and n- doping (with holes and electrons as majority carriers, respectively) would have similar characteristics. Therefore, if one adapts carbon nanotubes to MOSFET type architecture, in an inverter configuration the characteristics of the PMOS (p-type MOS) and the NMOS (n-type MOS) devices would be similar, which is a *distinct* advantage over silicon electronics. The possibility of easily p- or n-doping nanotubes (or of inter-conversion) through exposure to ambients (Section 2.2) is also an advantage. The FET architecture has been extended to
(i) a depletion mode type- where the CNT is fully doped,
(ii) an enhancement mode type- where carriers are induced in the CNT channel by an applied gate voltage, or
(iii) Schottky barrier type,[9] where a metal contact-nanotube interface regulates electrical transport.

Excellent reviews, studying such configurations for the application of nanotubes in electronics exist[6, 8, 9] and this section aims to take a brief but critical look at the advantages and drawbacks of using CNTs for transistor applications.

It is to be noted that as the band gap is inversely related to the diameter, (Section 2.1) only small diameter MWNTs are used for electrical switching/transistor related applications. CNT transistors, in the FET configurations above, have been used to demonstrate complex logic circuits[154–156] and memory[157] applications.

The use of nanotubes in FET type has a few peculiar merits, especially in terms of reducing the leakage current and minimizing the power- two issues of vital importance in the scaling of transistor devices, in accordance with ITRS (International Technology Roadmap for Semiconductors) recommendations.[158] A few other innovations, in addition to smaller device size,[159] could also occur as a consequence, *viz.,*
(a) the possibility of moving away from the SiO_2/Si interface paradigm- an issue of importance in terms of the ever reducing oxide thickness in silicon electronics. Alternative dielectric materials, such[49] HfO_2 or ZrO_2, can now be used with higher gate capacitance and improved performance.
(b) The chemical inertness of the nanotube surface is also advantageous in terms of reducing surface recombination, leakage current, and sub-threshold conduction.[160]
(c) Lower resistance (or higher transconductance) in the devices, due to the reduced effects of phonon scattering in low dimensional nanostructures. This can lead to faster device operation coupled with low power dissipation.

However, interface traps and inefficient contacts are often seen to plague CNT based transistors and affect the device characteristics significantly. The ambient oxygen also affects the device performance by inadvertently doping the contacts/nanotube. While the defects can, in some cases be exploited (say, a charged impurity can gate the device forming a *localized* diode)[161] in most instances this represents a loss of control and a source of unreliability. This leads one to the conclusion that CNT based transistors are

unlikely to find immediate application in large scale electronics. However, an *individual* nanotube transistor's superior performance and sensitivity over a silicon FET can be used in niche applications such as sensors. As an example, the chemical stability of a SWNT FET was exploited[162] in a salt-water environment, where the electrolyte potential was used to gate the nanotube conduction. As the FET is immersed, the gating efficiency is higher and the device can be used at low voltages (up to an order of magnitude lower than in vacuum) with conceivable single molecule sensitivity.

8.1.3. High Frequency Electronics

A scientific topic of great interest in the study of SWNTs is Luttinger liquid behavior (Section 2.1) and its possible consequences. In such a system, the creation of an electron is equivalent to the excitation of an infinite number of one-dimensional plasmons.[163] The generation of these plasmons led to the evaluation of high frequency properties, performance, and applications of SWNTs along with their possible use in nanometer sized antennae,[164] detectors, and mixers.[165]

The high mobilities,[51] large transconductances, and long mean free paths (>1 μm) of nanotubes promise their application in high frequency electronics. *Intrinsic* to an isolated SWNT, the frequency scales are set by the (a) $(RC)_{int}$ time constant and, (b) the combined effects of the capacitance and transconductance (g_m). $(RC)_{int}$ can be as small as 25 femtoseconds (corresponding to a minimum resistance of 6.3 kΩ i.e., $h/4e^2$ and a capacitance value of 0.1 aF) with a corresponding frequency of 6.3 THz ($= \frac{1}{(2\pi RC)}$). The quantity $\frac{g_m}{2\pi C_{gs}} (= f_T)$ corresponds to the highest frequency at which current gain is possible and for a g_m of 10 μS we obtain[166] an ultimate limit of operation of 0.4 THz. While *extrinsic* circuits and parasitics reduce the frequencies of operation from the intrinsic limits above, the operating speeds are nevertheless, still very impressive.

In radio-frequency (RF) applications, a SWNT (of diameter d) referenced to a ground plane (at a distance h) can be modeled as a transmission line[167] with lumped impedances—electrostatic capacitance,

$$C_{ES} = \frac{2\pi\varepsilon}{\cosh^{-1}(2h/d)}, \sim 50 \text{ aF}/\mu\text{m}$$

and magnetic inductance,

$$\mathcal{L}_M = \frac{\mu}{2\pi}\cosh^{-1}\left(\frac{2h}{d}\right), 1pH/\mu m$$

where $\mu(=\mu_o\mu_r)$ and $\varepsilon(=\varepsilon_o\varepsilon_r)$ refer to the magnetic permeability and the dielectric constant respectively. However, in nanosystems, it also becomes necessary to consider the quantum capacitance (C_Q) and the kinetic inductance ($\mathcal{L}_K$),[168] which may even be more important than the classical electrostatics numbers. Considering the electron system in a nanotube as a quantum mechanical box/quantum dot (Section 2.4) it takes a finite energy to add one extra electron, which is taken into account by the C_Q, which in a one-dimensional system $= \frac{G_o}{v_F}$, and is calculated to be $\sim$100 aF/μm (G_o is the quantum of conductance $= \frac{2e^2}{h}$ and v_F the Fermi velocity, $\sim 8 \cdot 10^5$ m/s). The kinetic energy of the added electrons (only electrons above the Fermi level: E_F are considered) is taken into account through $\mathcal{L}_K = (G_o v_F)^{-1}$, which translates to $\sim$16 nH/μm. Considering all these quantities individually, one comes up with an equivalent transmission line model (neglecting electron spin), illustrated in Figure 18(a). (Generalizing the above expressions in the transmission line model where many (say, M) modes of transmission are operative, it can be derived that when M is of the order of the relative dielectric constant (ε_r), C_Q and L_K can be ignored and we recover the usual transmission line model).

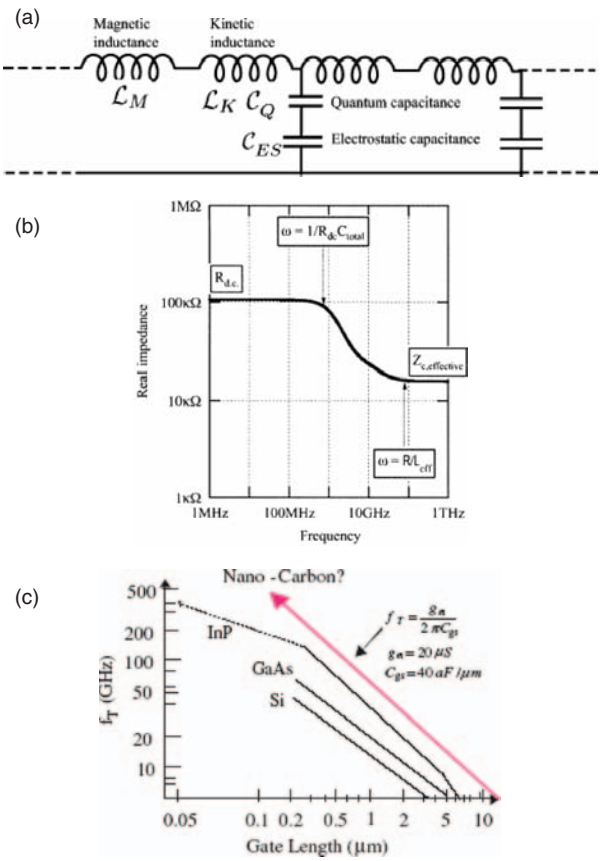

Fig. 18. (a) The reactive components of the impedance, including both the quantum and classical inductances and capacitances, must be taken into account for analyzing the performance of nanotubes in high frequency electronics, (b) The high frequency response of an SWNT with a roll-off dictated by the intrinsic nanotube resistance and parasitic effects, (c) The cut-off frequency (f_T) for reliable transistor performance has a considerably better scaling than conventional semiconductors. Reprinted with permission from [163], P. J. Burke, *IEEE Trans. Nanotech.* 1, 129 **(2002)**. © 2002, IEEE; [168] P. J. Burke, *IEEE Trans. Nanotech.* 2, 55 **(2003)**. © 2003, IEEE; [169], P. J. Burke, *Solid State Electron.* 48, 1981 **(2004)**. © 2004, Elsevier Ltd.

Considering the frequencies (ω) of operation (e.g., with a time scale set by the momentum relaxation time,

τ, $\sim 10^{-12}$ s), only at $\omega > \tau^{-1}$ the inductive impedance ($\sim \omega L_K$) is comparable to the series resistance, R. As seen earlier, this again corresponds to THz frequencies for SWNTs. However, external circuit connections also have to be taken into account and the overall characteristics are depicted through the frequency response of the dynamic impedance ($Z = R + j\omega\mathcal{L}$) of a 100 μm long metallic SWNT (Fig. 18(b)). Two points of inflexion are seen: the first point is determined by the RC time constant of the *external circuit* as $\omega_1 = 1/RC$ (typically ~0.5–5 GHz) while the second point $\omega_2 = R/\mathcal{L}$ (~10–50 GHz). Note that the larger of $\mathcal{L}_K$ or $\mathcal{L}_M$ dictates the overall inductance, while the smaller of C_{ES} or C_Q determines the capacitance of the nanotube device.

Considering the above factors, a small-signal equivalent model of a nanotube transistor has been proposed[166] which takes into account the finite gate-source capacitance (incorporating both C_{ES} and C_Q) of ~44 aF/μm, parasitic capacitance (~100 aF//μm), the transconductance and the series resistance. A f_T of 8 GHz was predicted in these approximations. Only by reducing the parasitics to negligible values, and in the ballistic limit, f_T is of the order of $\frac{80\ \text{GHz}}{L(\mu\text{m})}$ and with a nanotube, of sub-micron lengths (L) THz cut-off frequencies should be possible[169] (Fig. 18(c)).

However, in preliminary experimental work on the microwave transport[170] in metallic SWNTs through S-parameter measurements up to 10 GHz, no frequency dependence of the impedance (the DC response was identical to the AC response) or resonance effects were observed. This was attributed to the effects of resistance damping and optical phonon scattering in the CNTs. The small signal levels at high frequencies and the parasitic probe pad capacitance, which could be much larger than the intrinsic nanotube capacitance,[36] make sensitive measurements difficult. Typically, nanotube resistances are much higher than 50 Ω, which poses problems for a conventional[171] impedance-matched high frequency setup. Additionally, the fabrication of test circuits such as ring oscillators is non-trivial due to the difficulty of nanotube placement.

Alternate ways to explore the high-frequency characteristics include:
(1) Studying the small signal behavior through time-domain measurements using a high-impedance measurement system, while large signal measurements were carried out through frequency domain[36] analyses, and
(2) Exploiting the non-linear [172]/diode[165] like mixer characteristics of nanotube transistors.

In the time-domain measurements the bandwidth of the CNT device was inferred through pulsed measurements. A pulse with a short rise time was applied to the gate of the device and the rise time of the resulting output pulse, measured on an oscilloscope, was taken as a measure of the bandwidth. The impedances and parasitics of the measuring circuits and instruments, including the cables, the load resistor etc., must be carefully considered. Through such measurements a switching speed up to 100 kHz was measured, with the upper frequency restriction imposed by the measurement system.[36] In frequency domain measurements, the limitations, at high frequency, arise from the cross-talk between the gate and drain and attention must be paid to de-embedding the *true* FET signal. Fabricating the CNT FET on insulating quartz substrates partly alleviates this problem by lowering the overall cross-talk level. Such a measurement scheme permitted a response up to 100 MHz to be observed at an expense of reduced signal intensity (Fig. 19(a)). A roll-off of the frequency response was observed due to interference effects between the capacitively coupled cross-talk and the CNT-FET drain current. Future measurements would have to

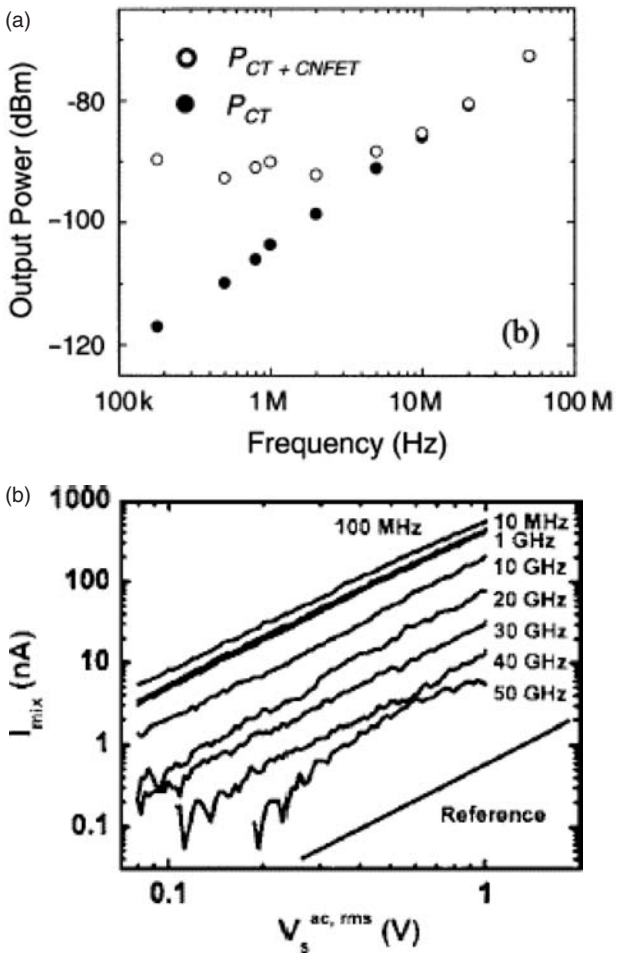

Fig. 19. (a) **Direct measurement** of 100 MHz operation of a nanotube FET. The figure shows the signal power from a nanotube field effect transistor (P_{CNFET}) along with crosstalk (P_{CT}) at high frequencies. Parasitics interfere with the direct measurement of the frequency characteristics and must be carefully de-embedded. Reprinted with permission from [36], D. V. Singh et al., *IEEE Trans. Nanotech.* 3, 383 (**2004**). © 2004, IEEE; (b) An **indirect measurement** of high frequency performance is through using the nanotube as a mixer.[171] A DC mixing current (I_{mix}) is obtained at frequencies up to 50 GHz, in response to an applied AC gate voltage, in a SWNT based FET. Reprinted with permission from [165], S. Rosenblatt et al., *Appl. Phys. Lett.* 87, 153111 (**2005**). © 2005, American Institute of Physics.

devise strategies on avoiding these parasitic behaviors. An indirect observation of high frequency operation up to 580 MHz[172] was made by observing the DC current response of the nanotube to a combined AC/DC signal. For a device/CNT transistor exhibiting non-linear I–V characteristics, a change in the DC current proportional to the amplitude of the applied AC voltage is observed. These measurements showed that the response was essentially frequency independent in a large domain (250 kHz–580 MHz) over a range (0–0.5 V) of AC voltages (it was noted that the upper limit, of 580 MHz, was again due to the limitations of the measurement setup and does not represent an intrinsic value).

Yet another indirect measurement of nanotube response to frequency was made by using a SWNT transistor as a mixer. When a combined DC bias voltage (V_o) along with a small signal RF voltage ($v_o \cos \omega t$) is fed into a non-linear device, a fraction of the RF input signal is converted to DC power[171] along with a rectified/DC current of magnitude $\frac{v_o^2}{4} G'_d$ where G'_d is the derivative of the conductance with respect to the voltage (N.B. This rectification is also followed by higher harmonic AC signals which can be filtered out). This DC current is obtained at frequencies (ω_o) smaller than $(RC)^{-1}$ (the inverse time constant of the transistor). In this experiment, a high resistivity Si substrate was used for the CNT transistor and measurements were performed in vacuum to minimize any variation of the gate voltage threshold voltage. Interestingly, there was a small overlap ($\sim$100 nm) of the top gate contact[165] (which was used for the mixing) with the source electrode. Mixing up to 50 GHz (Fig. 19(b)) was observed (the RC time constant of the device was consequently estimated to be $\sim$100 ps) with an upper limit set by the external measuring circuit at 100 GHz. Again, the frequency measurement of only up to 50 GHz was due to the frequency source limitations and *not* the CNT device.

Further *direct* measurements at higher frequencies (>1 GHz)[170] are necessary to explore the detailed behavior of nanotubes and their LL characteristics. However, indirect observations using the non-linear properties of the nanotube devices promise their use for high frequency electronics.

8.1.3.1 Nanotube Antennae. The impedance mismatch between nanotubes ($\sim$kΩ) and macroscopic RF circuitry and packaging (50 Ω) poses an interfacing problem in nano-devices. One way around this problem is to construct a system completely out of nanotubes (Section 7). Yet another way is *wireless* contact through nanotube antennae. The radiation pattern for a CNT is comparable to that of a small dipole (Section 6) as the size is small relative to the free-space wavelength (λ_0).

A comparison[173] of metallic nanotubes with conventional[171] metallic dipole antennae reveals significant differences due to (1) Additional impedances (C_Q and $\mathscr{L}_K$—see Section 8.1.3), and (2) associated plasmonic effects. In a conventional microstrip configuration, the boundary conditions imply a vanishing longitudinal electric field, at the edges. However, in a one-dimensional SWNT conductor, the field does not completely vanish due to the quantum inductance ($\mathscr{L}_K$) related to electron inertia. Consequently, plasmonic dispersion effects have been predicted in waveguide,[174] which propagate along the surface and length of the tube with a reduced velocity,

$$u(\sim 0.02c) = \sqrt{\frac{1}{\mathscr{L}_{\text{total}} C_{\text{total}}}} \left(= \sqrt{\frac{\frac{1}{C_{ES}} + \frac{1}{C_Q}}{\mathscr{L}_K + \mathscr{L}_M}} \right)$$

These plasmon resonances are only active above the relaxation frequency ($f_{rel} = 1$/relaxation time) and their velocity is larger than the Fermi velocity (v_F). For a large length (l) to diameter (d) aspect ratio it was derived[173] that nanotube dipoles exhibit sharp resonances with a wavelength of $\lambda_p (= 0.01\lambda_o$, the free space wavelength), which can be modified[175] by periodic scatterers, e.g., by filling the interior of the nanotubes with a material of a different permittivity. The distinctly different current distribution on nanotubes, due to the λ_p modulation, has the effect of dramatically reducing the efficiencies (P_{rad}/P_{in} of $\sim 10^{-5}$) through increased surface resistance losses compared to a copper based nano-antenna. The gain (G), proportional to the product of the efficiency and directivity (D, $\sim$1.5), is consequently very small. However, in the nano-regime, these efficiencies might be adequate for assessing electromagnetic interactions and nano-device communications.

8.2. CNTs as Field Emitters

A currently used application of carbon nanotubes in the commercial arena,[176] exploiting their nanometer scale radius of curvature is their use as field emitter arrays in displays. When employed as electron emitters, there is a large enhancement factor (β) in the field emission, and emission can be obtained at a lower threshold voltage.[177] This increased sensitivity to electrical fields can be used for example, in gas ionization sensors.[178] Other applications include micron scale on-chip triodes for high frequency (>200 MHz)[179] vacuum microelectronics, and X-ray generation.[180] The use of CNTs in cold cathode devices allows for

(i) instantaneous turn-on,
(ii) high power,
(iii) low control voltage operation, along with long lifetimes and miniaturization.

Compared to thermionic emission, field emission induced from nanotubes also offers the additional advantages of lower power consumption and room temperature operation.

For a metal with a flat surface, the threshold electric field for field emission can be large, at 10^4 V/μm which is impractical. In CNTs however, β (the field enhancement factor which is the ratio of the electric field at the CNT

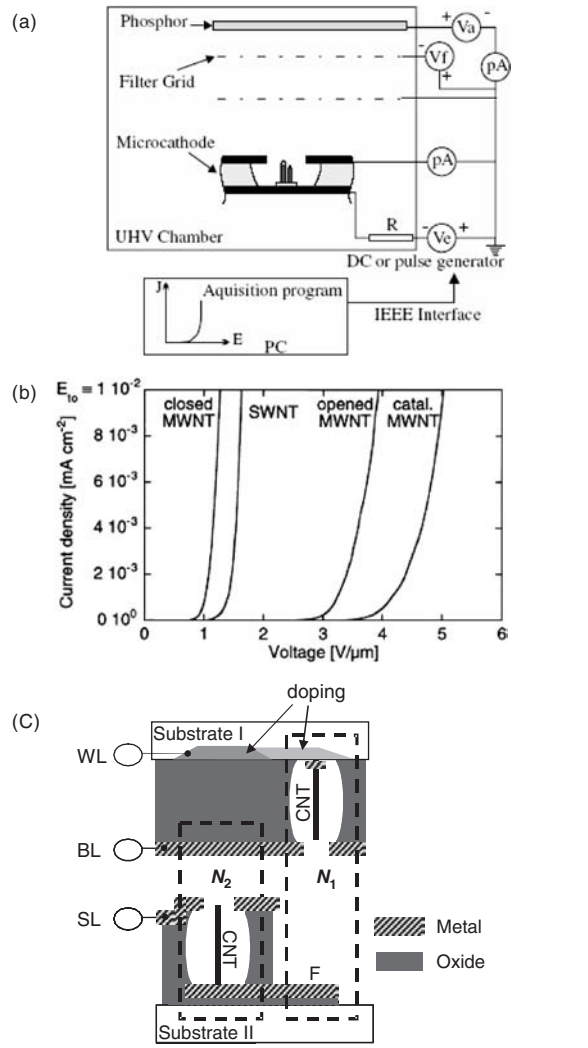

Fig. 20. (a) A typical triode-like setup to measure field emission with the carbon nanotube used as the cathode. Reprinted with permission from [189], G. Pirio et al., *Nanotechnology* 13, 1 **(2002)**. © 2002, IOP Publishing Ltd.; (b) The relative efficiencies of field emission from various types/configurations of nanotubes, as a function of turn-on voltage. Reprinted with permission from [185], J.-M. Bonard et al., *Appl. Phys. A* 69, 245 **(1999)**. © 1999, Springer-Verlag; (c) Schematic of a non-volatile memory based on CNT field emission. Reprinted with permission from [192], J. P. Hollingsworth and P. Bandaru, *Appl. Phys. Lett.* 87, 23315 **(2005)**. © 2005, American Institute of Physics.

tip and the macroscopic electric field and a function of tip geometry) can be as high[177] as 3000, with orders of magnitude lower turn-on voltages (<10 V/μm),[181] and larger currents (up to 1 μA from a single MWNT)[182] and current densities ($\sim$200 mA/cm^2).

Regulated field emission can be obtained from the tips of metallic nanotubes, in a triode-like arrangement, where the CNT functions as the cathode (Fig. 20(a)). The emission current (I) is determined by the Fowler-Nordheim relationship:

$$I = AV^2 \exp\left(-\frac{b\phi^{3/2}}{\beta V}\right)$$

where V is the applied voltage, ϕ the work-function of the surface ($\sim$4.8 eV for a CNT,[183] and which can be reduced by adsorbates[184] and Cs intercalation)[183] and a and b are phenomenological constants. While it would be expected that vertically orientated CNTs have the best emission characteristics, the effect of screening between individual nanotube emitters must also be taken into account.[181] For nanotube of length L, radius r, and spaced a distance s apart, β approximates to

$$1.2\left(\frac{L}{r}+2.15\right)^{0.9}\left[1-\exp\left(\frac{-2.3172s}{L}\right)\right]$$

Experimentally,[185] the turn-on ($E_{to} < 2$V/μm) and the threshold-fields ($E_{thr} < 5$V/μm) for metallic nanotube field emitters was seen to be lower by a factor of two than comparable geometries, e.g., CVD diamond on silicon-tips. It was also determined that both the internal geometry of the nanotubes as well as their placement was important in their field emission characteristics. Generally, SWNT films, due to a higher degree of structural perfection, had the highest β(>3000) while catalytically grown MWNTs had a β approaching 800- which could be ascribed to their larger tip radius. Most single *open* (where the tip was removed by oxidation)[185]/*closed* MWNTs are capable of emitting over a large current range (from 10 pA–0.2 mA). However, the efficiency of emission is lower for the open tubes in terms of a two-fold increase in the threshold voltage (Fig. 20(b)) Aligned MWNTs were also found to have a larger density of states (DOS) and a lower work function than the randomly oriented MWNTs due to a difference in the distribution of their electronic states.[186]

It has also been demonstrated through electron holography studies[187] that the electric field is concentrated only at the CNT tips and not at any surrounding defects. Other important characteristics of field emission from CNTs include a smaller electron energy spread ($\sim$0.2 eV) compared to metallic electron emitters ($\sim$0.45 eV). The discreteness of the electronic energy levels was posited to be the reason, associated with which a field emission induced luminescence, from localized states at the tips, was also observed. The quantum efficiency (= the ratio of emitted photons to field emitted electrons) of the luminescence was $\sim 10^{-6}$. The majority contribution to the emission arises from states at/near the Fermi energy (E_F), which in turn depends on the tube geometry, presence of defects etc. It was predicted, through electronic structure calculations,[65] that the optimum geometry for field emission corresponds to a *slant-cut* open CNT with dangling bonds of the zigzag type which contribute the highest density of localized states. A compilation of field emission characteristics from various nanotube structures has been presented.[188]

Several experimental realizations of carbon nanotubes in aligned field emitter configuration[177, 189–191] have been made, in which the Fowler Nordheim relation was verified and electron emission obtained. The specific values of

the turn-on voltages vary with the experimental arrangement. The reliability of CNT emitters in terms of current decay is of interest, and could be due to tip blunting, caused by bombardment from surrounding ions and/or carbon evaporation. When such issues are resolved it is very likely that CNT based field emitters can be used in applications such as X-ray sources and field emission displays which require high currents (>100 mA) coupled with large integration densities (>10^5 emitters/cm^2) with low power consumption. It has also been proposed[192] to use carbon-nanotube based field emission in a vacuum microelectronics based non-volatile memory core. A design that can be implemented with state-of-the art nanotube fabrication techniques is shown in Figure 20(c) and nonvolatile memory operation, up to 0.25 GHz, has been shown to be feasible through circuit simulations. When integrated with flip-chip technology, this type of memory offers a possible solution to the problem of flash memory scaling coupled with the advantages of high density integrated circuitry and a faster speed of operation.

8.3. Bio-Chemical Sensors, Through the Measurement of Changes in Electrical Conductivity

In view of their high carrier mobilities and chemical sensitivity, field effect transistor (FET) devices with carbon nanotubes as the conducting channel have been used to detect changes in the surrounding electrochemical potential. Note that the chemical inertness of SWNTs makes covalent attachment difficult and physisorbtion/non-covalent attraction is a more likely mechanism for analyte binding.[193] On the other hand, the surfaces of nanotubes can also be manipulated, for chemical sensing, by appropriate functionalization to achieve specificity. As an example, a helical configuration of the streptavidin protein, useful in many biochemical assays, can be crystallized[194] on a MWNT surface through size and *hydrophobic* effects.[195] It is also possible to attach carboxylic acid groups resulting in a *hydrophilic* nanotube surface which prevents protein attachment.[196] Non-covalent binding to anchor a bio-receptor molecule onto a nanotube has also been attempted.

A FET can also be configured, without a gate,[197] in which case the analyte can deplete/accumulate carriers in the channel and cause an electrical property change through *chemical gating*. Sensors exploiting such changes in the electrical characteristics of nanotubes have been used both in gas and liquid environments. An example of an effort in using *semiconducting* SWNTs (metallic SWNTs have much less sensitivity) in gas sensors is the work by Kong[198] et al., where a three orders of magnitude change in the electrical resistance was observed on exposure to oxidizing and reducing gases such as NO_2 and NH_3 with a sensitivity of 2 ppm and 0.1% respectively. The rationale for the experimental results hinged on electrical modification of the doping of intrinsic p-type nanotubes (with holes as majority carriers). While strong oxidizers (say, NO_2) resulted in a charge transfer *from* the SWNT, an opposite effect (charge transfer *to* the nanotube) was observed with reducing agents (say, NH_3). Consequently, in the former case, an increased hole density results with enhanced electrical conductivity while electron donation to the p-type SWNT results in a decreased conductance. It is to be noted that similar principles could account for a transition from p- to n-type conductivity, on exposure to a reducing atmosphere (Section 2.2) From basic organic chemistry,[199] it would also appear that the activating (due to –OH, –NH_x, –CH_3 etc.) or deactivating (due to halogens, –NO_2, –COOH, –CN etc.) effects of substituents and functionalizing agents on the nanotube could also play a major influence and a careful control of the ambient would be necessary for

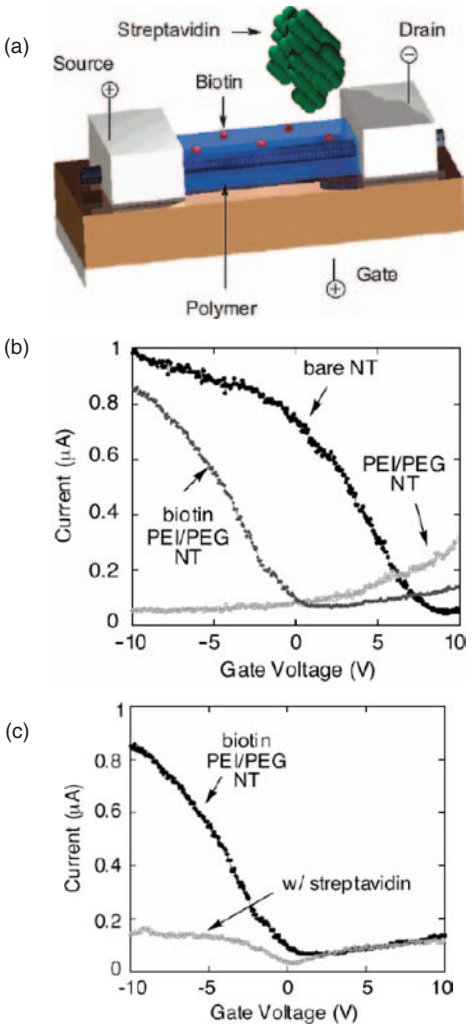

Fig. 21. (a) A schematic of a nanotube FET configuration that can be used to detect protein binding/bio-sensing via the interaction of the streptavidin protein with surface immobilized biotin. The polymer coating is used to preserve the physical properties of the nanotube. (b) The *I–V* characteristics of the FET are specific to the chemical entity being detected; the effect of the biotin assembly on the PEI/PEG coated nanotube electrical characteristics is distinct and can be used to initialize the sensor, (c) The binding of streptavidin to biotin manifested in the electrical conducting characteristics. Reprinted with permission from [196], A. Star et al., *Nano lett.* 3, 459 **(2003)**. © 2003, The American Chemical Society.

interpreting experimental results. It was recently[200] suggested that hitherto observed conductivity changes of the nanotube were not intrinsic. One also needs to consider the influence of the gases/environment on the electrodes, and consequently modifying sensor characteristics.[200] Through electrical field distribution simulations such effects were taken into account,[200] through changes in the contact metal work function and their influence on the Schottky barrier constituting the transistor. Another interesting explanation of the experimental results hypothesizes that the nanotube only serves as a counter—electrode in the measurement scheme.[201] The influence of mobile ions on nanotube FET characteristics in an aqueous environment[202] provides support for this argument.

A few applications of chemical sensing in an aqueous environment include the specific detection of protein binding,[196] exploiting the well known biotin-streptavidin interactions on to a polymer (a mixture of polyetheleneimine-PEI for n-doping the nanotube[193] and polyethylene glycol-PEG for inducing a hydrophilic surface) coated nanotube arranged in a FET configuration (Fig. 21(a)). The Current—Gate voltage (V_g) characteristics from a bare nanotube indicate a change from p-type behavior to n-type on PEI coating (Fig. 21(b)). On immobilizing biotin on the polymer surface, the covalent binding reduces the overall electron concentration and the device characteristics revert to p-type. On streptavidin attachment the conductance is reduced considerably (Fig. 21(c)) which indicates the onset of detection. While the current detection level is around ten streptavidin molecules higher sensitivity can be achieved through a better control of the surface charges. In another interesting application, the fast electron transfer rate and the high electro catalytic effect, intrinsic to CNTs, was used[203] for the fabrication of glucose sensors. Several other biosensors for detecting a whole host of pathogens and chemicals are also being developed with the nanotube as a base element.[204]

The small scale of the sensing element, in the form of a nanotube, could enable high sensitivity and the change of the electrical properties of a nanotube can be used in the future for electronic sensing at the cellular level and *in-vivo* physiological studies.

9. OUTLOOK FOR THE FUTURE

This review has aimed to give an overview of the extensively studied topic of the electrical properties of nanotubes. The outstanding message is that the reduced dimensionality, inherent to nanotubes, gives rise to new physical effects in which quantum mechanical considerations are important. This marks a departure from classical electromagnetic phenomena and devices, and also represents a large opportunity for future technological advancement. As CNTs can be synthesized both as metallic and semiconducting forms, this feature can be used to make heterogeneous metal-semiconductor junctions or homogeneous metal-metal/semiconductor-semiconductor junctions, and this can be extensively exploited in device design. In this section, the obstacles to be overcome for fruition of promising CNT based applications at the frontiers of electronic technology will be discussed.

In the short term, CNTs could provide an example of a disruptive technology for interconnect applications and heat management, i.e., when tightly packed so as to have the same cross-sectional area[33] as copper interconnect (Section 8.1.1) nanotubes have been found to have lower resistivity and higher resistance to electromigration failure. The ability of SWNT field effect transistors in biosensing is also likely to engender new applications in view of the nanotubes' chemical and mechanical stability. A higher density of integration of CNTs is necessary for their extensive application in Field emission displays. The wide variety of electrical phenomena exhibited by CNTs can be optimally harnessed through the creation of a multifunctional device (powered by thermoelectric effects) for autonomous sensing.

In the longer term, the prognosis is less clear. While integration of CNT growth with silicon CMOS[205] and flexible polymer[206] substrates has been demonstrated as an example of top-down and bottom-up integration, in our view this represents an evolutionary advance. Silicon technology, over the years, has proven to be very robust and adaptable and CNTs could be embraced into the Silicon fold as another nanostructured material.

In order for CNTs to stand on their own and be extensively used in nanoelectronics, it is necessary to provide for their controlled and rational growth in place of the random assembly in vogue. While efforts in this direction have been proliferating, they seem to have not kept pace with the rapid advances in the science of nanotubes. Such a chasm is being perceived as being detrimental to the deployment of nanotubes in the commercial/industrial arena, which is essential for continued growth. Synthesis and fabrication methods should also incorporate efficient means for

(i) distinct growth of metallic and semiconducting nanotubes, and

(ii) their rapid assembly at a scale/rate comparable to what is possible for silicon technologies.

A fundamental analysis of what new technologies/devices are possible in reduced dimensions, using nanotubes, is then needed. A few such examples are the recent analyses of the high frequency properties[163] and array-based architectures[5] for nanotube based electronics. While it is likely that the CNT field is still relatively young, forays in such directions are necessary and would greatly contribute to its vitality. We look forward to ideas along the lines of Conway and Mead's classic textbook[207] applied to nanotubes and nanosystems integration.

Novel and different device architectures would also be necessary to exploit the unique CNT properties and bring forth new devices. One possible example, using Y-and

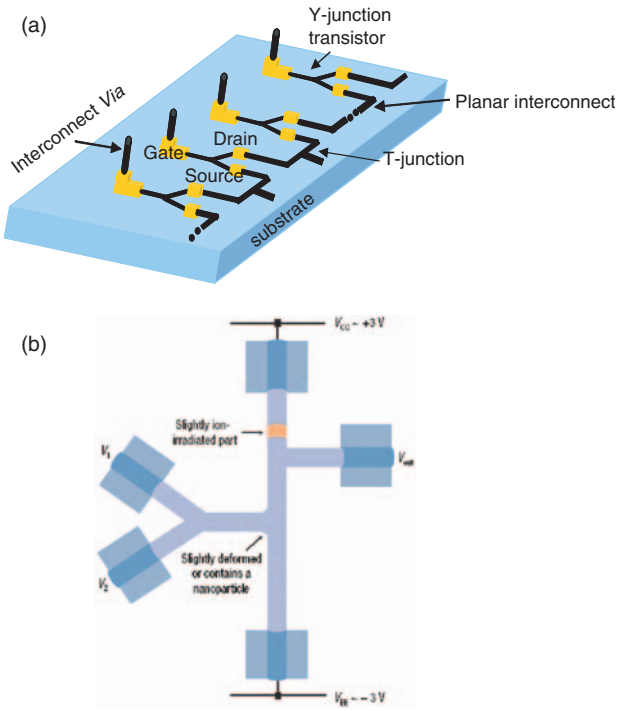

Fig. 22. A conceptual view of a possible CNT technology platform, including novel carbon morphologies (such as Y- and T-junctions), interconnect *vias* and directed nanotube growth. Such, three-dimensional nano-interconnected designs can go beyond existing technologies (MOSFET etc.) and bring forth new functionalities. (b) A proposed logic circuit (XNOR logic) based on Y- and T-junction CNT topology. V_1 and V_2 represent the inputs while the output terminal is V_{out}. Reprinted with permission from [151], H. Q. Xu, *Nat. Mater.* 4, 649 **(2005)**. © 2005, Nature Magazine.

T-junctions is illustrated in Figure 22. This would lead to new paradigms in device electronics design. It would also be desirable, in the future to fabricate an integrated nanotube architecture, where all the components, i.e., the connections as well as the logic and memory devices are fabricated from nanotubes. This could have immediate practicability in high frequency electronics, where the electrode geometry in conventional designs causes complications in measurements and applications. The parasitic capacitances in an integrated nanotube configuration could potentially be smaller[166] and result in THz scale operating speeds. While the road to achieving such architectures might be hard and long, the rewards and insights it would bring could be many-fold.

Acknowledgments: The author gratefully acknowledges support from the National Science Foundation (Grant ECS-05-08514 and the Office of Naval Research (Award number N00014-06-1-0234).

References and Notes

1. R. H. Baughman, A. A. Zakhidov, and W. A. de Heer, *Science* 297, 787 **(2002)**.
2. P. L. McEuen, *Nature* 393, 15 **(1998)**.
3. P. Avouris, *Acc. Chem. Res.* 35, 1026 **(2002)**.
4. M. J. Kelly, Low-Dimensional Semiconductors, Oxford University Press, New York **(1995)**.
5. A. DeHon, First Workshop on Non-Silicon Computation, 1, **(2002)**.
6. P. L. McEuen, M. S. Fuhrer, and H. Park, *IEEE Trans. Nanotech.* 1, 78 **(2002)**.
7. P. L. McEuen and J.-Y. Park, *MRS Bulletin* 29, 272 **(2004)**.
8. P. Avouris, J. Appenzeller, R. Martel, and S. Wind, *Proc. IEEE* 91, 1772 **(2003)**.
9. J. Appenzeller, J. Knoch, R. Martel, and V. Derycke, *IEEE Trans. Nanotech.* 1, 184 **(2002)**.
10. P. G. Collins and P. Avouris, *Scientific American*, 62, **(2000)**.
11. Z. Yao, C. Dekker, and P. Avouris, Electrical Transport through Single-Wall Carbon Nanotubes, Springer-Verlag, Heidelberg **(2001)**.
12. H. Dai, Nanotube Growth and Characterization, Topics in Applied Physics, Springer-Verlag, Berlin **(2001)**, Vol. 80, p. 29.
13. K. B. K. Teo, C. Singh, M. Chhowalla, and W. I. Milne, Catalytic Synthesis of Carbon Nanotubes and Nanofibers, Encyclopedia of Nanoscience and Nanotechnology, edited by H. S. Nalwa, American Scientific Publishers, Stevenson Ranch, CA **(2004)**.
14. A. V. Melechko, V. I. Merkulov, T. E. McKnight, M. A. Guillorn, K. L. Klein, D. H. Lowndes, and M. L. Simpson, *J. Appl. Phys.* 97, 041301 **(2005)**.
15. E. Joselevich and C. M. Lieber, *Nano lett.* 2, 1137, **(2002)**.
16. Y. Zhang, A. Chang, J. Cao, Q. Wang, W. Kim, Y. Li, N. Morris, E. Yenilmez, J. Kong, and H. Dai, *Appl. Phys. Lett.* 79, 3155 **(2001)**.
17. S. G. Rao, L. Huang, W. Setyawan, and S. Hong, *Nature* 425, 36 **(2003)**.
18. Y. Huang, X. Duan, Q. Wei, and C. M. Lieber, *Science* 291, 630 **(2001)**.
19. J. Kong, H. T. Soh, A. M. Cassell, C. F. Quate, and H. Dai, *Nature* 395, 878 **(1998)**.
20. X. M. H. Huang, R. Caldwell, L. Huang, S. C. Jun, M. Huang, M. Y. Sfeir, S. P. O'Brien, and J. Hone, *Nano lett.* 5, 1515 **(2005)**.
21. P. M. Ajayan, *Chem. Rev.* 99, 1787 **(1999)**.
22. C. Kittel, Introduction to Solid State Physics, 7th edn., John Wiley, New York **(1995)**.
23. J. W. Mintmire, B. I. Dunlap, and C. T. White, *Phys. Rev. Lett.* 68, 631 **(1992)**.
24. N. Hamada, S. Sawada, and A. Oshiyama, *Phys. Rev. Lett.* 68, 1579 **(1992)**.
25. R. Saito, M. Fujita, G. Dresselhaus, and M. S. Dresselhaus, *Appl. Phys. Lett.* 60, 2204 **(1992)**.
26. Z. Yao, C. Dekker. and P. Avouris, Electrical Transport through Single-Wall Carbon Nanotubes, Carbon Nanotubes: Synthesis, Structure, Properties, and Applications, edited by M. S. Dresselhaus, G. Dresselhaus, and P. Avouris, Springer-Verlag GmbH, Heidelberg **(2001)**, Vol. 80, p. 147.
27. L. Forro and C. Schonenberger, Physical properties of Multi-wall Nanotubes, Carbon Nanotubes, Topics in Applied Physics, edited by M. S. Dresselhaus, G. Dresselhaus, and P. Avouris, Springer-Verlag, Heidelberg **(2001)**.
28. K. Liu, M. Burghard, S. Roth, and P. Bernier, *Appl. Phys. Lett.* 75, 2494 **(1999)**.
29. J. Voit, *Reports of Progress in Physics* 58, 977 **(1995)**.
30. R. Egger and A. O. Gogolin, *Phys. Rev. Lett.* 79, 5082 **(1997)**.
31. M. Bockrath, D. H. Cobden, J. Lu, A. G. Rinzler, R. E. Smalley, L. Balents, and P. L. McEuen, *Nature* 397, 598 **(1999)**.
32. M. S. Fuhrer, J. Nygard, L. Shih, M. Forero, Y.-G. Yoon, M. S. C. Mazzoni, H. J. Choi, J. Ihm, S. Louie, A. Zettl, and P. L. McEuen, *Science* 288, 494 **(2000)**.
33. S. Salahuddin, M. Lundstrom, and S. Datta, *IEEE Trans. Elec. Dev.* 52, 1734 **(2005)**.
34. P. Delaney, H. J. Choi, J. Ihm, S. G. Louie, and M. L. Cohen, *Nature* 391, 466 **(1998)**.
35. S. J. Tans, A. R. M. Verschueren, and C. Dekker, *Nature* 393, 49 **(1998)**.

36. D. V. Singh, K. A. Jenkins, J. Appenzeller, D. Neumayer, A. Grill, and H.-S. P. Wong, *IEEE Trans. Nanotech.* 3, 383 **(2004)**.
37. V. Derycke, R. Martel, J. Appenzeller, and P. Avouris, *Appl. Phys. Lett.* 80, 2773 **(2002)**.
38. A. M. Rao, P. C. Eklund, S. Bandow, A. Thess, and R. E. Smalley, *Nature* 388, 257 **(1997)**.
39. D. C. J. Sorescu, K. D., P. Avouris, *J. Phys. Chem. B* 105, 11227 **(2001)**.
40. R. Czerw, M. Terrones, J.-C. Charlier, X. Blase, B. Foley, R. Kamalakaran, N. Grobert, H. Terrones, D. Tekleab, P. M. Ajayan, W. Blau, M. Ruhle, and D. L. Carroll, *Nano lett.*, 1, 457 **(2001)**.
41. S. M. Sze, Physics of Semiconductor Devices, John Wiley, New York **(1981)**.
42. F. Leonard and J. Tersoff, *Phys. Rev. Lett.* 83, 5174 **(1999)**.
43. M. A. Pimenta, A. Marucci, S. D. M. Brown, M. J. Matthews, A. M. Rao, P. C. Eklund, R. E. Smalley, G. Dresselhaus, and M. S. Dresselhaus, *J. Mater. Res.* 13, 2396 **(1998)**.
44. M. S. Dresselhaus, G. Dresselhaus, and A. Jorio, *Annual Review of Materials Research* 34, 247 **(2004)**.
45. M. Freitag, M. Radosavljevic, Y. Zhou, and A. T. Johnson, *Appl. Phys. Lett.* 79, 3326 **(2001)**.
46. S. Datta, Electronic Transport in Mesoscopic Systems, Cambridge University Press, New York **(1995)**.
47. M. J. Madou, Fundamentals of Microfabrication, CRC Press, New York **(2002)**.
48. A. Bachtold, M. Henny, C. Terrier, C. Strunk, C. Schönenberger, J.-P. Salvetat, J.-M. Bonard, and L. Forro, *Appl. Phys. Lett.* 73, 274 **(1998)**.
49. J. Guo, S. Datta, M. Lundstrom, B. M., P. L. McEuen, A. Javey, H. Dai, H. Kim, and P. McIntyre, Assessment of Silicon MOS and Carbon Nanotube FET Performance Limits Using a General Theory of Ballistic Transistors, IEDM Meeting, San Francisco, CA **(2002)**, 711.
50. R. Martel, T. Schmidt, H. R. Shea, T. Hertel, and P. Avouris, *Appl. Phys. Lett.* 73, 2447 **(1998)**.
51. X. Zhou, J.-Y. Park, S. Huang, J. Liu, and P. L. McEuen, *Phys. Rev. Lett.* 95, 146805 **(2005)**.
52. A. Javey, J. Guo, Q. Wang, M. Lundstrom, and H. Dai, *Nature* 424, 654 **(2003)**.
53. W. Liang, M. Bockrath, D. Bozovic, J. H. Hafner, M. Tinkham, and H. Park, *Nature* 411, 665 **(2001)**.
54. M. Bockrath, D. H. Cobden, P. L. McEuen, N. G. Chopra, A. Zettl, A. Thess, and R. E. Smalley, *Science* 275, 1922 **(1997)**.
55. S. J. Tans, M. H. Devoret, H. Dai, A. Thess, R. E. Smalley, L. J. Geerligs, and C. Dekker, *Nature* 386, 474 **(1997)**.
56. J. Nygard, D. H. Cobden, M. Bockrath, P. L. McEuen, and P. E. Lindelof, *Appl. Phys. A* 69, 297 **(1999)**.
57. M. Buitelaar and T. N. A. Bachtold, M. Iqbal, and C. Schönenberger, *Phys. Rev. Lett.* 88, 156801 **(2002)**.
58. P. Jarillo-Herrero, S. Sapmaz, C. Dekker, L. P. Kouwenhoven, and H. S. J. van der Zant, *Nature* 429, 389 **(2004)**.
59. S. J. Tans, M. H. Devoret, R. J. A. Groeneveld, and C. Dekker, *Nature* 394, 761 **(1998)**.
60. D. H. Cobden, M. Bockrath, P. L. McEuen, A. G. Rinzler, and R. E. Smalley, *Phys. Rev. Lett.* 81, 681 **(1998)**.
61. S. J. Tans and C. Dekker, *Nature* 404, 834 **(2000)**.
62. P. L. McEuen, M. Bockrath, D. H. Cobden, Y.-G. Yoon, and S. Louie, *Phys. Rev. Lett.* 83, 5098 **(1999)**.
63. R. Saito, G. Dresselhaus, and M. S. Dresselhaus, *J. Appl. Phys.* 73, 494 **(1993)**.
64. P. G. Collins, M. S. Arnold, and P. Avouris, *Science* 292, 706 **(2001)**.
65. S. Han and J. Ihm, *Phys. Rev. B* 61, 9986 **(2000)**.
66. S. C. Tsang, Y. K. Chen, P. J. F. Harris, and M. L. H. Green, 372, 159 **(1994)**.
67. C. Schonenberger, A. Bachtold, C. Strunk, J.-P. Salvetat, and L. Forro, *Appl. Phys. A* 69, 283 **(1999)**.
68. A. Bachtold, C. Strunk, J.-P. Salvetat, J.-M. Bonard, L. Forro, T. Nussbaumer, and C. Schonenberger, *Nature* 397, 673 **(1999)**.
69. R. Saito, G. Dresselhaus, and M. S. Dresselhaus, *J. Appl. Phys.* 73, 494 **(1992)**.
70. C.-H. Kiang, M. Endo, P. M. Ajayan, G. Dresselhaus, and M. S. Dresselhaus, *Phys. Rev. Lett.* 81, 1869 **(1998)**.
71. Y.-K. Kwon and D. Tomanek, *Phys. Rev. B* 58, R16001 **(1998)**.
72. S. Frank, P. Poncharal, Z. L. Wang, and W. A. de Heer, *Science* 280, 1744 **(1998)**.
73. H. J. Li, W. G. Lu, J. J. Li, X. D. Bai, and C. Z. Gu, *Phys. Rev. Lett.* 95, 086601 **(2005)**.
74. L. Langer, V. Bayot, E. Grivei, J.-P. Issi, J. P. Heremans, C. H. Olk, L. Stockman, C. Van Haesendonck, and Y. Bruynseraede, *Phys. Rev. Lett.* 76, 479 **(1996)**.
75. S. N. Song, X. K. Wang, R. P. H. Chang, and J. B. Ketterson, *Phys. Rev. Lett.* 72, 697 **(1994)**.
76. K. Liu, P. Avouris, R. Martel, and W. K. Hsu, *Phys. Rev. B* 63, 161404 **(2001)**.
77. P. A. Lee, A. D. Stone, and H. Fukuyama, *Phys. Rev. B* 35, 1039 **(1987)**.
78. L. X. Benedict, V. H. Crespi, S. G. Louie, and M. L. Cohen, *Phys. Rev. B* 52, 14935 **(1995)**.
79. M. Tinkham, *Introduction to Superconductivity*, Dover Publications Inc., Mineola, NY **(2004)**.
80. M. Kociak, A. Y. Kasumov, S. Gueron, B. Reulet, I. I. Khodos, Y. B. Gorbatov, V. T. Volkov, L. Vaccarini, and H. Bouchiat, *Phys. Rev. Lett.* 86, 2416 **(2001)**.
81. Z. K. Tang, L. Zhang, N. Wang, X. X. Zhang, G. H. Wen, G. D. Li, J. N. Wang, C. T. Chan, and P. Sheng, *Science* 292, 2462 **(2001)**.
82. A. Y. Kasumov, R. Deblock, M. Kociak, B. Reulet, H. Bouchiat, I. I. Khodos, Y. B. Gorbatov, V. T. Volkov, C. Journet, and M. Burghard, *Science* 284, 1508 **(1999)**.
83. A. F. Morpurgo, J. Kong, C. M. Marcus, and H. Dai, *Science* 286, 263 **(1999)**.
84. L. D. Hicks and M. D. Drsselhaus, *Phys. Rev. B* 47, 16631 **(1993)**.
85. R. Venkatasubramanian, E. Siivola, T. Colpitts, and B. O'Quinn, *Nature* 413, 597 **(2001)**.
86. G. Mahan and J. O. Sofo, *Proc. Nat. Acad. Sci.* 93, 7436 **(1996)**.
87. G. D. Mahan, Thermoelectric Power of Carbon Nanotubes, Taylor and Francis, New York **(2006)**.
88. K. Schwab, E. A. Hendriksen, J. M. Worlock, and M. L. Roukes, *Nature* 404, 974 **(2000)**.
89. J. S. Tse and D. Klug, Recent Trends for the Design and Optimization of Thermoelectric Materials-A Theoretical Perspective, Thermoelectrics Handbook: Macro to Nano, CRC Press, Boca Raton, **(2006)**.
90. M. D. Dresselhaus, Y. M. Lin, M. R. Black, O. Rabin, and G. Dresselhaus, New Directions for Low Dimensional Thermoelectricity, *Materials Research Society Symposium Proceedings*, edited by G. S. Nolas, J. Yang, T. P. Hogan, and D. C. Johnson, MRS, Boston, MA **(2003)**, Vol. 793.
91. D. A. Broido and T. L. Reinecke, *Appl. Phys. Lett.* 70, 2834 **(1997)**.
92. Z. Sun, Z. Zhang, and M. S. Dresselhaus, *Appl. Phys. Lett.* 74, 4005 **(1999)**.
93. J. Hone, I. Ellwood, M. M., A. Mizel, M. L. Cohen, A. Zettl, A. G. Rinzler, and R. E. Smalley, *Phys. Rev. Lett.* 80, 1042 **(1998)**.
94. L. Grigorian, G. U. Sumanasekera, A. L. Loper, S. L. Fag, A. J. L., and P. C. Eklund, *Phys. Rev. B* 60, R11309 **(1999)**.
95. J. P. Small, L. Shi, and P. Kim, *Solid State Commun.* 127, 181 **(2003)**.
96. P. Kim, L. Shi, A. Majumdar, and P. L. McEuen, *Phys. Rev. Lett.* 87, 215502 **(2001)**.
97. J. P. Small, K. M. Perez, and P. Kim, *Phys. Rev. Lett.* 91, 256801 **(2003)**.
98. W. Yi, L. Lu, D. L. Zhang, Z. W. Pan, and S. S. Xie, *Phys. Rev. B* 59, R9015 **(1999)**.

99. S. Berber, Y.-K. Kwon, and D. Tomanek, *Phys. Rev. Lett.* 84, 4613 **(2000)**.
100. G. Chen et al., *J. Nanoparticle Res.* 2, 199 **(2000)**.
101. M. J. Biercuk, M. C. Llaguno, M. Radosavljevic, J. K. Hyun, A. T. Johnson, and J. E. Fischer, *Appl. Phys. Lett.* 80, 2767 **(2002)**.
102. T. E. Humphrey and H. Linke, *Phys. Rev. Lett.* 94, 096601 **(2005)**.
103. C. Dekker, *Physics Today* 22, **(1999)**.
104. A. Jorio, R. Saito, T. Hertel, R. B. Weisman, G. Dresselhaus, and M. S. Dresselhaus, *MRS Bulletin* 29, 276 **(2004)**.
105. Y. Wang, K. Kempa, B. Kimball, J. B. Carlson, G. Benham, W. Z. Li, P. Ke, T., J. Rybcynski, J. Herczynski, and Z. F. Ren, *Appl. Phys. Lett.* 85, 2607 **(2004)**.
106. A. Jorio, M. A. Pimenta, A. G. Souza Filho, G. G. Samsonidze, A. K. Swan, M. S. Unlu, B. B. Goldberg, R. Saito, G. Dresselhaus, and M. S. Dresselhaus, *Phys. Rev. Lett.* 90, 107403 **(2003)**.
107. W. A. de Heer, W. S. Bacsa, A. Chatelain, T. Gerfin, R. Humphrey-Baker, L. Forro, and D. Ugarte, *Science* 268, 845 **(1995)**.
108. T. G. Pedersen, *Phys. Rev. B* 67, 073401 **(2003)**.
109. X. Qiu, M. Freitag, V. Perebeinos, and P. Avouris, *Nano lett.* 5, 749 **(2005)**.
110. G. N. Ostojic, S. Zaric, J. Kono, V. C. Moore, R. H. Hauge, and R. E. Smalley, *Phys. Rev. Lett.* 94, 097401 **(2005)**.
111. C. R. J., N. R. Franklin, J. Kong, J. Cao, T. W. Tombler, Y. Zhang, and H. Dai, *Appl. Phys. Lett.* 79, 2258 **(2001)**.
112. M. J. O'Connell, S. M. Bachilo, C. B. Huffman, V. C. Moore, M. S. Strano, E. H. Haroz, K. L. Rialon, P. J. Boul, W. H. Noon, C. Kittrell, J. Ma, R. H. Hauge, R. B. Weisman, and R. E. Smalley, *Science* 297, 593 **(2002)**.
113. M. Freitag, Y. Martin, J. A. Misewich, R. Martel, and P. Avouris, *Nano lett.* 3, 1067 **(2003)**.
114. J. A. Misewich, R. Martel, P. Avouris, J. C. Tsang, S. Heinze, and J. Tersoff, *Science* 300, 783 **(2003)**.
115. J. Chen, V. Perebeinos, M. Freitag, J. Tsang, Q. Fu, J. Liu, and P. Avouris, *Science* 310, 1171 **(2005)**.
116. M. Freitag, V. Perebeinos, J. Chen, A. Stein, J. C. Tsang, J. A. Misewich, R. Martel, and P. Avouris, *Nano lett.* 4, 1063 **(2004)**.
117. M. Freitag, J. Chen, J. Tersoff, J. C. Tsang, Q. Fu, J. Liu, and P. Avouris, *Phys. Rev. Lett.* 93, 076803 **(2004)**.
118. J. Hone, M. C. Laguno, N. M. Nemes, A. T. Johnson, J. E. Fischer, D. A. Walters, M. J. Casavant, J. Schmidt, and R. E. Smalley, *Appl. Phys. Lett.* 77, 666 **(2000)**.
119. P. Delaney, M. Di Ventra, and S. Pantelides, *Appl. Phys. Lett.* 75, 3787 **(1999)**.
120. H. W. C. Postma, T. Teepen, Z. Yao, M. Grifoni, and C. Dekker, *Science* 293, 76 **(2001)**.
121. P. R. Bandaru, C. Daraio, S. Jin, and A. M. Rao, *Nat. Mater.* 4, 663 **(2005)**.
122. J.-M. Ting and C.-C. Chang, *Appl. Phys. Lett.* 80, 324 **(2002)**.
123. P. G. Collins, M. Hersam, M. Arnold, R. Martel, and P. Avouris, *Phys. Rev. Lett.* 86, 3128 **(2001)**.
124. J. O. Wesstrom, *Phys. Rev. Lett.* 82, 2564 **(1999)**.
125. D. Zhou and S. Seraphin, *Chem. Phys. Lett.* 238, 286 **(1995)**.
126. W. Z. Li, J. G. Wen, and Z. F. Ren, *Appl. Phys. Lett.* 79, 1879 **(2001)**.
127. C. Papadapoulos, A. Rakitin, J. Li, A. S. Vedeneev, and J. M. Xu, *Phys. Rev. Lett.* 85, 3476 **(2000)**.
128. B. C. Satishkumar, P. J. Thomas, A. Govindaraj, and C. N. R. Rao, *Appl. Phys. Lett.* 77, 2530 **(2000)**.
129. K. Tsukagoshi, E. Watanabe, I. Yagi, N. Yoneya, and Y. Aoyagi, *New J. Phys.* 6, 1 **(2004)**.
130. T. Palm and L. Thylen, *Appl. Phys. Lett.* 60, 237 **(1992)**.
131. L. Worschech, H. Q. Xu, A. Forchel, and L. Samuelson, *Appl. Phys. Lett.* 79, 3287 **(2001)**.
132. R. Lewen, I. Maximov, I. Shorubalko, L. Samuelson, L. Thylen, and H. Q. Xu, *J. Appl. Phys.* 91, 2398 **(2002)**.
133. K. Hieke and M. Ulfward, *Phys. Rev. B.* 62, 16727 **(2000)**.
134. I. Shorubalko, H. Q. Xu, P. Omling, and L. Samuelson, *Appl. Phys. Lett.* 83, 2369 **(2003)**.
135. A. M. Song, A. Lorke, A. Kriele, J. P. Kotthaus, W. Wegscheider, and M. Bichler, *Phys. Rev. Lett.* 80, 3831 **(1998)**.
136. A. N. Andriotis, M. Menon, D. Srivastava, and L. Chernozatonski, *Phys. Rev. Lett.* 87, 066802 **(2001)**.
137. A. N. Andriotis, D. Srivastava, and M. Menon, *Appl. Phys. Lett.* 83, 1674 **(2003)**.
138. W. Tian, S. Datta, S. Hong, R. Reifenberger, J. I. Henderson, and C. P. Kubiak, *J. Chem. Phys.* 109, 2874 **(1998)**.
139. V. Meunier, M. B. Nardelli, J. Bernholc, T. Zacharia, and J.-C. Charlier, *Appl. Phys. Lett.* 81, 5234 **(2002)**.
140. S. Heinze, J. Tersoff, R. Martel, V. Derycke, J. Appenzeller, and P. Avouris, *Phys. Rev. Lett.* 89, 106801 **(2002)**.
141. J. H. Davies, The Physics of Low-Dimensional Semiconductors, Cambridge University Press, New York **(1998)**.
142. H. Q. Xu, *Appl. Phys. Lett.* 80, 853 **(2001)**.
143. D. Csontos and H. Q. Xu, *Phys. Rev. B* 67, 235322 **(2003)**.
144. H. Q. Xu, *Physica E* 13, 942 **(2002)**.
145. T. Palm and L. Thylen, *J. Appl. Phys.* 79, 8076 **(1996)**.
146. M. B. Nardelli, B. I. Yakobson, and J. Bernholc, *Phys. Rev. Lett.* 81, 4656 **(1998)**.
147. V. H. Crespi, *Phys. Rev. B* 58, 12671 **(1998)**.
148. N. Gothard, C. Daraio, J. Gaillard, R. Zidan, S. Jin, and A. M. Rao, *Nano lett.* 4, 213 **(2004)**.
149. M. Terrones, F. Banhart, N. Grobert, J.-C. Charlier, H. Terrones, and P. M. Ajayan, *Phys. Rev. Lett.* 89, 075505 **(2002)**.
150. A. M. Song, P. Omling, L. Samuelson, W. Seifert, I. Shorubalko, and H. Zirath, *Appl. Phys. Lett.* 79, 1357 **(2001)**.
151. H. Q. Xu, *Nat. Mater.* 4, 649 **(2005)**.
152. W. Steinhogl, G. Schindler, G. Steinlesberger, M. Traving, and M. Engelhardt, *J. Appl. Phys.* 97, 023706 **(2005)**.
153. M. Ohring, Reliability and Failure of Electronic Materials and Devices, Academic Press, San Diego **(1998)**.
154. A. Bachtold, P. Hadley, T. Nakanishi, and C. Dekker, *Science* 294, 1317 **(2001)**.
155. V. Derycke, R. Martel, J. Appenzeller, and P. Avouris, *Nano lett.* 1, 453 **(2001)**.
156. R. Martel, V. Derycke, J. Appenzeller, S. Wind, and P. Avouris, Carbon Nanotube Field-Effect Transistors and Logic Circuits, New Orleans, LA **(2002)**.
157. M. S. Fuhrer, B. K. Kim, T. Durkop, and T. Brintlinger, *Nano lett.* 2, 757 **(2002)**.
158. http://public.itrs.net/, International Technology Roadmap for Semiconductors, **(2005)**.
159. R. V. Seidel, A. P. Graham, J. Kretz, B. Rajasekharan, G. S. Duesberg, M. Liebau, E. Unger, F. Kreupl, and W. Hoenlein, *Nano lett.* 5, 147 **(2005)**.
160. R. S. Muller and T. I. Kamins, Device Electronics for Integrated Circuits, John Wiley, New York **(1986)**.
161. R. D. Antonov and A. T. Johnson, *Phys. Rev. Lett.* 83, 3274 **(1999)**.
162. S. Rosenblatt, Y. Yaish, J. Park, J. Gore, V. Sazonova, and P. L. McEuen, *Nano lett.* 2, 869 **(2002)**.
163. P. J. Burke, *IEEE Trans. Nanotech.* 1, 129 **(2002)**.
164. P. J. Burke, C. Rutherglen, and Z. Yu, *International Journal of High Speed Electronics Systems* **(2006)**.
165. S. Rosenblatt, H. Lin, V. Sazonova, S. Tiwari, and P. L. McEuen, *Appl. Phys. Lett.* 87, 153111 **(2005)**.
166. P. J. Burke, *Carbon Nanotube Devices for GHz to THz Applications, Proceedings of the 2003 International Semiconductors Device Research Symposium*, **(2003)**.
167. S. Ramo, J. R. Whinnery, and T. van Duzer, Fields and Waves in Communication Electronics, New York **(1993)**.
168. P. J. Burke, *IEEE Trans. Nanotech.* 2, 55 **(2003)**.
169. P. J. Burke, *Solid State Electron.* 48, 1981 **(2004)**.
170. Z. Yu and P. J. Burke, *Nano lett.* 5, 1403 **(2005)**.

171. D. M. Pozar, Microwave Engineering, John Wiley and Sons, Inc., New York **(1998)**.
172. J. Appenzeller and D. J. Frank, *Appl. Phys. Lett.* 84, 1771 **(2004)**.
173. G. W. Hanson, *IEEE Trans Antenn. Propag.* 53, 3426 **(2005)**.
174. J.-O. Wesstrom, *Phys. Rev. B* 54, 11484 **(1996)**.
175. G. Y. Slepyan, S. A. Maksimenko, A. Lakhtakia, O. Yevtushenko, and A. V. Gusakov, *Phys. Rev. B* 60, 17136 **(1999)**.
176. J. H. Choi, A. R. Zoulkarneev, Y. W. Jin, Y. J. Park, D. S. Chung, B. K. Song, I. T. Han, H. W. Lee, S. H. Park, H. S. Kang, H. J. Kim, J. W. Kim, J. E. Jung, J. M. Kim, H. G. Baek, and S. G. Yu, *Appl. Phys. Lett.* 84, 1022 **(2004)**.
177. Y. Cheng and O. Zhou, *C. R. Phys.* 4, 1021 **(2003)**.
178. A. Modi, N. Koratkar, E. Lass, B. Wei, and P. M. Ajayan, *Nature* 424, 171 **(2003)**.
179. C. Bower, W. Zhu, D. Shalom, D. Lopez, L. H. Chen, P. L. Gammel, and S. Jin, *Appl. Phys. Lett.* 80, 3820 **(2002)**.
180. G. Z. Yue, Q. Qiu, B. Gao, Y. Cheng, J. Zhang, H. Shimoda, S. Chang, J. P. Lu, and O. Zhou, *Appl. Phys. Lett.* 81, 355 **(2002)**.
181. S. H. Jo, Y. Tu, Z. P. Huang, D. L. Carnahan, D. Z. Wang, and Z. F. Ren, *Appl. Phys. Lett.* 82, 3520 **(2003)**.
182. A. G. Rinzler, J. H. Hafner, P. Nikolaev, L. Lou, S. G. Kim, D. Tomanek, P. Nordlander, D. T. Colbert, and R. E. Smalley, *Science* 269, 1550 **(1995)**.
183. S. Suzuki, C. Bower, Y. Watanabe, and O. Zhou, *Appl. Phys. Lett.* 76, 4007 **(2000)**.
184. A. Maiti, J. Andzelm, N. Tanpipat, and P. von Allmen, *Phys. Rev. Lett.* 87, 155502 **(2001)**.
185. J.-M. Bonard, J.-P. Salvetat, T. Stockli, L. Forro, and A. Chatelain, *Appl. Phys. A* 69, 245 **(1999)**.
186. S. Suzuki, Y. Watanabe, T. Kiyokura, K. G. Nath, T. Ogino, S. Heun, W. Zhu, C. Bower, and C. Zhou, *Phys. Rev. B* 63, 245418 **(2001)**.
187. J. Cummings, A. Zettl, M. R. McCartney, and J. C. H. Spence, *Phys. Rev. Lett.* 88, 056804 **(2002)**.
188. M. Sveningsson, R.-E. Morjan, O. A. Nerushev, Y. Sato, J. Backstrom, E. E. B. Campbell, and F. Rohmund, *Appl. Phys. A* 73, 409 **(2001)**.
189. G. Pirio, P. Legagneux, D. Pribat, K. B. K. Teo, M. Chhowalla, G. A. J. Amaratunga, and W. I. Milne, *Nanotechnology* 13, 1 **(2002)**.
190. M. A. Guillorn, A. V. Melechko, V. I. Merkulov, E. D. Ellis, C. L. Britton, M. L. Simpson, D. H. Lowndes, and L. R. Baylor, *Appl. Phys. Lett.* 79, 3506 **(2001)**.
191. M. A. Guillorn, M. D. Hale, V. I. Merkulov, M. L. Simpson, G. Y. Eres, H. Cui, A. A. Puretzky, and D. B. Geohegan, *J. Vaccum. Sci. Tech. B* 21, 957 **(2003)**.
192. J. P. Hollingsworth and P. Bandaru, *Appl. Phys. Lett.* 87, 23315 **(2005)**.
193. H. Dai, *Acc. Chem. Res.* 35, 1035 **(2002)**.
194. F. Balavoine, P. Schultz, C. Richard, V. Mallouh, T. W. Ebbesen, and C. Mioskowski, *Angew. Chemie. Intl. Edn.* 38, 1912 **(1999)**.
195. R. J. Chen, Y. Zhang, D. Z. Wang, and H. Dai, *J. Am. Chem. Soc.* 123, 3838 **(2001)**.
196. A. Star, J.-C. P. Gabriel, K. Bradley, and G. Gruner, *Nano lett.* 3, 459 **(2003)**.
197. Y. Cui, Q. Wei, H. Park, and C. M. Lieber, *Science* 293, 1289 **(2001)**.
198. J. Kong, N. R. Franklin, C. Zhou, M. G. Chapline, S. Peng, K. Cho, and H. Dai, *Science* 287, 622 **(2000)**.
199. R. T. Morrison and R. N. Boyd, Organic Chemistry, Allyn and Bacon Inc., Boston **(1983)**.
200. S. Heinze, J. Tersoff, R. Martel, V. Derycke, J. Appenzeller, and P. Avouris, *Phys. Rev. Lett.* 89, 106801 **(2002)**.
201. P. L. McEuen, Materials Research Society, Fall 2005 meeting, **(2005)**.
202. K. Bradley, J. Cumings, A. Star, J.-C. P. Gabriel, and G. Gruner, *Nano lett.* 3, 639 **(2003)**.
203. Y. Lin, F. Lu, Y. Tu, and Z. Ren, *Nano lett.* 4, 191 **(2004)**.
204. C. R. Martin and P. Kohli, *Nature* 2, 29 **(2003)**.
205. Y.-C. Tseng, P. Xuan, A. Javey, R. Malloy, Q. Wang, J. Bokor, and H. Dai, *Nano lett.* 4, 123 **(2004)**.
206. M. C. McAlpine, R. S. Friedman, and C. M. Lieber, *Proc. IEEE* 93, 1357 **(2005)**.
207. C. Mead and L. Conway, Introduction to VLSI Systems, Addison-Wesley, Menlo Park, CA **(1980)**.
208. J.-M. Ting and C.-C. Chang, *Appl. Phys. Lett.* 80, 324 **(2002)**.
209. G. E. Scuseria, *Chem. Phys. Lett.* 195, 534 **(1992)**.
210. A. N. Andriotis, M. Menon, D. Srivastava, and L. Chernozatonski, *Phys. Rev. B* 65, 165416 **(2002)**.

Received: 30 January 2006. Revised/Accepted: 27 May 2006.